On the role of the axial ligand in heme proteins: a theoretical study

Rydberg, Patrik; Sigfridsson, Emma; Ryde, Ulf

Published in:
Journal of Biological Inorganic Chemistry

DOI:
10.1007/s00775-003-0515-y

2004

Document Version:
Peer reviewed version (aka post-print)

On the role of the axial ligand in haem proteins – a theoretical study

Patrik Rydberg, Emma Sigfridsson & Ulf Ryde

Department of Theoretical Chemistry

Lund University

Chemical Centre, P. O. Box 124

S-221 00 Lund, Sweden

Correspondence to U. Ryde

Phone: +46-46-222 45 02

Fax: +46-46-222 45 43

E-mail: Ulf.Ryde@teokem.lu.se

2017-04-09

Abstract

We present a systematic investigation of how the axial ligand in haem proteins influences the geometry, electronic structure, and spin states of the active site, and the energies of the reaction cycles. Using the density functional B3LYP method and medium-sized basis sets, we have compared models with His, His+Asp, Cys, Tyr, and Tyr+Arg as is found in myoglobin and haemoglobin, peroxidases, cytochrome P450, and haem catalases, respectively. We have studied twelve reactants and intermediates of the reaction cycles of these enzymes, including complexes with H_2O, OH^-, O^{2-}, CH_3OH, O_2, H_2O_2, and HO_2^- in various formal oxidation states of the iron ion (II to V). The results show that His gives ~0.6 V higher reduction potentials than the other ligands. In particular, it is harder to reduce and protonate the O_2 complex with His than with the other ligands, in accordance with the O_2 carrier function of globins and the oxidative chemistry of the other proteins. For most properties, the trend Cys < Tyr < Tyr+Arg < His+Asp < His is found, reflecting the donor capacity of the various ligands. Thus, it is easier to reduce compound I with a His+Asp ligand than with a Cys ligand, in accordance with the one-electron chemistry of peroxidases and the hydroxylation reactions of cytochromes P450. However, the Tyr complexes have an unusually low affinity for all neutral ligands, giving them a slightly enhanced driving force in the oxidation of H_2O_2 by compound I.

Keywords: Cytochrome P450, peroxidase, catalase, myoglobin, density functional calculations

Introduction

Haem is one of the most important coenzymes in biology, being employed in a large number of proteins with functions ranging from electron transfer (cytochromes) to the binding and transport of small molecules (e.g. O_2 in myoglobin and haemoglobin) and the catalysis of a great wealth of reactions (e.g. peroxidases, oxidases, and catalases) [1,2].

Haem consists of an iron ion bound to the four central nitrogen atoms of a porphyrin ring. One or two axial ligands complete the octahedral coordination around the iron ion. These axial ligands vary extensively between different groups of haem proteins and it is believed that they tune the properties of the iron ion [3]. In the electron carriers, the protein provides two axial ligands (typically histidine or methionine), which ensure a low-spin state of the iron ion and a low reorganisation energy of the site [4]. In the globins, the protein provides only one axial ligand, histidine (His), whereas the opposite side is open for O_2 binding [1,2]. Likewise, the surrounding protein provides only one axial ligand in the haem enzymes, whereas the sixth site is open for the substrate.

Interestingly, even among the haem enzymes, the protein-derived axial ligand varies with the function. Thus, all cytochromes P450 [5], as well as chloroperoxidase [6] and NO synthase [7], have a cysteine (Cys) haem ligand, whereas all peroxidases have a His ligand [8], and all haem catalases have a tyrosine (Tyr) ligand [9]. This has led to extensive investigations of the influence of the axial ligand on the reactivity of the haem site [3,10-13].

It has been realised that not only the first-sphere ligands of the iron ion are important for the properties, but also some second-sphere ligands. For example, the His ligand forms a hydrogen bond to an aspartate (Asp) residue in all peroxidases [8], and this interaction is believed to impose an imidazolate character of the His ligand, thereby increasing the electron density on the iron ion [3]. This may be an important source of the differing reactivity of peroxidases and globins, which share the same axial ligand, but the hydrogen bond to Asp is replaced by weaker hydrogen bonds to back-bone carbonyl groups in the globins. Likewise, the Tyr ligand in haem catalases is invariably hydrogen bonded to an arginine (Arg) residue [9], which probably also tunes the reactivity of this site [14].

The reaction cycles of haem enzymes have many similarities. Cytochromes P450 catalyse the stereospecific hydroxylation of non-activated hydrocarbons, a reaction that uncatalysed requires extremely high temperatures to proceed even unspecificly [15-17]. The most widely accepted reaction cycle of the P450 enzymes is shown in Figure 1 [5,15-18]. In the resting state (**1**), the haem site is six-coordinate low-spin Fe^{III}, with a water molecule as the sixth ligand. The reaction cycle starts with binding of the substrate, which leads to the dissociation of the water molecule and a transition to the high-spin state (**2**), although the substrate does not coordinate directly to the iron ion. A one-electron reduction transforms the ion to high-spin Fe^{II} (**3**), which subsequently binds O_2 (**4**). The addition of another electron gives a complex (**5**) that takes up a proton to form a hydroperoxide intermediate (**6**; sometimes called compound 0). If another proton is added to this complex, the O–O bond breaks and a water

molecule dissociates from the site, leaving a highly reactive Fe^{V}=O (formally) intermediate (**7**). This is *compound I*, which is believed to be the active catalytic intermediate that has the potential to hydroxylate most substrates. It is widely supposed that the reaction proceeds via a hydrogen-atom abstraction, followed by rebound of the organic radical to the Fe^{IV}–OH intermediate (**8**), giving a Fe^{III}–alcohol complex (**9**) [8,19]. The substitution of water for the product completes the reaction cycle.

Peroxidases share a similar reaction cycle. However, they are mainly five-coordinate in the resting state (**2**), and this state is never reduced. Instead, it binds H_2O_2 (**10**), which is deprotonated to the hydroperoxide intermediate (**6**) and then reprotonated on the distal oxygen atom to form compound I (**7**) in a manner similar to cytochrome P450. Moreover, in the peroxidases, the iron-bound oxygen atom is not available to the substrate, which instead binds close to the edge of the haem group [8]. Therefore, peroxidases instead abstract an electron from the substrate, forming a Fe^{IV}=O (formally) intermediate, *compound II* (**11**). This complex can abstract an electron from another substrate molecules, thereby returning to the resting state (**2**) after the uptake of two protons and the dissociation of a water molecule. No intermediates have been observed in this step, but it has lately been suggested that compound II may be protonated to Fe^{IV}–OH [20,21], which is identical to the hydrogen-abstraction intermediate (**8**) in the P450 reaction. We have also included the one-electron reduced Fe^{III}–OH complex (**12**) in our study.

Finally, the reaction cycle of haem catalases is similar to that of the peroxidases, involving a five-coordinate Fe^{III} resting state (**2**), binding of H_2O_2 (**10**), and the formation of compound I (**7**) via a hydroperoxide intermediate (**6**). However, in the catalases, compound I binds another molecule of H_2O_2 which is oxidised to O_2 directly in a two-electron step without any observed intermediates [9]. Thus, catalases catalyse the disproportionation of two molecules of the toxic H_2O_2 to two molecules of water and and one molecule of O_2.

A natural way to probe the effect of the axial ligand in haem proteins is to use site-directed mutagenesis. This method has extensively been used, e.g. in myoglobin [22-25], haem oxygenase (which also has a His ligand, hydrogen-bonded only to back-bone carbonyl groups) [26], peroxidases [27-31], cytochrome P450 [32-36], chloroperoxidase [37], and cytochrome *c* [38]. Although some of the mutations have a low stability or fail to bind haem, the general result of the mutagenesis studies is that a negatively charged axial ligand (Cys, Tyr, or His+Asp) decreases the reduction potential and that at least a Cys ligand enhances P450-type activity. Likewise, second-sphere hydrogen bonds to the Cys ligand tend to increase the reduction potential, confirming the suggestion that it is connected to the electron density on the iron ion [36]. On the other hand, if the Asp group in peroxidase is mutated to aspargine, the activity decreases by a factor of 5 [30].

However, two findings have called in question the importance of the axial ligand for the activity of the haem proteins [10]. First, a His mutant of chloroperoxidase has almost full (60–80%) activity, showing that the native Cys ligand has little effect on the catalytic properties of

the protein [37]. Second, the almost full activity of a glutamine mutant of peroxidase, indicates that an imidazolate character of the native His ligand is not necessary for its function [27].

Another important source of information about the influence of the axial ligand is the study of haem model compounds [17,39-41]. It has been shown that thiolate ligation promotes O–O heterolysis compared to imidazole and chloride ligands [17,39,41], whereas hydrogen bonds to the thiolate ligand reduces this effect [3]. Other experiments indicate that a hydrogen bond to a carboxylate group increases heterolysis [42].

A third source of information is theoretical calculations. Many quantum chemical studies have been presented for the reaction intermediates of cytochrome P450, in particular for the electronic structure of compound I (**7**) and its reaction with various substrates [19,43-87]. Somewhat fewer theoretical studies have been performed on histidine models, mostly on the five-coordinate Fe(II) state (**2**), the O_2 adduct (**4**), and on compounds I and II (**7** and **8**) [47,49,62,66,71,80,81,85,86,88-111]. However, only a few studies have been performed on real peroxidase models with a hydrogen-bonded carboxylate group [47,89,107,111,112], whereas some authors have studied the limiting effect of an imidazolate ligand [47,62,80,91,108,113]. All these studies have concentrated on compound I (**7**). Finally, only five studies of catalase have been presented, all of compounds I or II (**7** or **11**); four with a realistic phenolate ligand and one with a CH_3O^- ligand [14,80,111,113,114]. Some investigators have compared the properties of various axial ligands [47,49,62,71,80,81,111,114,115], but most of them have been restricted to a comparison of the electronic structure of compound I (and II). However, it has been shown that thiolate models give a lower barrier for hydroxylation reactions than imidazole [47,81] and that the axial ligand affects the formation of compound I and the Fe(II/III) reduction potential [49].

The effect of the axial ligand in haem enzymes has traditionally been discussed in terms of the *push–pull* concept, originally formulated for peroxidases [116]. It suggests that the heterolytic reactivity of the peroxidases comes partly from the axial ligand (the push), especially from its hydrogen bond to the Asp group, which increases the negative charge of the ligand and the charge density on iron, thereby stabilising the high oxidation states in compounds I and II [62]. The other part of the reactivity (the pull) comes from the opposite (distal) side of the porphyrin ring, which contains His and Arg residues, which further enhance the heterolytic reactivity. In cytochrome P450, the softer Cys ligand gives an even stronger push, which makes the distal pull unnecessary (there are not polar residues on the distal side in these proteins) [117]. Thus, the most common views are that the axial ligand has a clear effect on reduction potentials, it probably stabilises compound I (and II), but it has a relatively minor effect on the O–O bond fission [3,117]. It has also been suggested that the most important effect of the axial ligand is to inhibit reformation of H_2O_2 from the hydroperoxide complex [36]. However, no consensus seems to have been reached yet.

In this paper, we present a systematic comparison of the four types of axial ligands

encountered in catalases, cytochrome P450, globins, and peroxidases, i.e. Tyr+Arg, Cys, His, and His+Asp. The comparison is based on density-functional calculations, in which we exploit the possibility to isolate the active haem site from the protein, thereby separating the direct effects of the axial ligand from effects caused by the surrounding protein, including the distal site. Thus, we pinpoint the effects of the axial ligand in a pure and unbiased way. We compare spin states, electronic structures, geometries, and relative energies of all intermediates in the reaction cycles of haem enzymes (complexes **1–12** in Figure 1). Thereby, we obtain some further clues about the influence of the axial ligand on the reactivity of the haem proteins. As a by-product, we also provide the first complete study of the reaction intermediates of catalases.

Methods

Quantum chemical geometry optimisations were performed with the density functional method B3LYP (unrestricted formalism for open-shell systems), as implemented in the Turbomole software [118,119]. Hybrid density functional methods have been shown to give as good or better geometries as correlated ab initio methods for first-row transition metal complexes [120,121] and the B3LYP method in particular seems to give the most reliable results among the widely available density functional methods [120-122]. In all calculations, we have used for iron the double-ζ basis set of Schäfer et al. (62111111/33111/311) [123], enhanced with one *f*, one *d*, and two *p* functions with exponents 1.339, 0.1244, 0.134915, and 0.041843, respectively. For the other atoms, we have employed the 6-31G* basis set, except for oxygen, for which we used the larger 6-31+G* basis (not on the Tyr or Asp models), with an additional diffuse function [124]. Only the pure 5 *d* and 7 *f*-type functions were used.

Calculations at this level of theory have been shown to give accurate results; for example, the calculated iron–ligand bond lengths in cytochrome models are only 2–3 (N_{Por}), 3 (S_{Cys}), and 4–5 pm (N_{His}) longer than those observed experimentally [4]. Calibrations have also shown that geometries obtained with this approach do not change much when the basis set is increased [125]. The full geometry of all models was optimised until the change in energy between two iterations was below 10^{-6} Hartree (2.6 J/mole) and the maximum norm of the internal gradients was below 10^{-3} a.u.. No symmetry restrictions or other constrains were imposed, unless otherwise stated.

We have modelled the active site of the haem proteins by iron porphine (Por; a porphyrin ring without any substituents) with one or two axial ligands. Several studies of haem proteins have indicated that the porphyrin side chains have a minor influence on the structure [48,65,126]. Recently, a QM/MM study of the reaction mechanism of cytochrome P450 indicated that a main contribution to the catalysis comes from the interaction between the propionate side chains and positively charged groups in the protein [127]. However, this is of less interest in the present comparison, where we want to concentrate on the intrinsic properties of the haem group with various axial ligands and disregard the atomic detail of the

surrounding protein. As the protein-derived axial ligand, we have used SCH_3^-, as a model of Cys[1], imidazole, as a model of His, phenolate as a model of Tyr, a methylguanidium ion $CH_3NHC(NH_2)_2^+$ as a model Arg, and acetate as a model of Asp. In the His–Asp hydrogen bond, the shared proton can reside both on His or Asp (HisH+Asp or His+HAsp). If not otherwise stated, it is assumed that it resides on Asp (which can be seen as the limiting case where the His ligand has been deprotonated to imidazolate). Both protonation states have been studied for models **2**–**7**. We will see that the reaction energies are quite insensitive to the exact location of the shared proton. The proton in the Tyr–Arg hydrogen bond always resides on Arg. As the sixth ligand, we used the full oxygen-derived molecule, H_2O, OH^-, O^{2-}, H_2O_2, HO_2^-, or O_2, CH_3OH (formally). Thus, we used the simplest possible model of an organic substrate, methanol. All twelve intermediates **(1–12)** shown in Figure 1 and described in the introduction were studied. Three spin states (high, intermediate, and low spin) were considered for the cysteine model and most of them also for the other axial ligands.

These quantum chemical calculations were performed in vacuum, whereas most reactions take place in water solution or in proteins. In order to study the effects of solvation, we have reoptimised the structures of all the most stable spin states in a solvent using the continuum conductor-like screening model (COSMO) [128], as implemented in Turbomole 5.5 [129]. These calculations were performed with default values for all parameters (implying a water-like probe molecule) and a dielectric constant of 80 and 4, to model pure water and to get a feeling of possible effects in a protein (where the effective dielectric constant is often estimated to be 2–16) [130,131]. For the atomic radii, we used the optimised COSMO radii in Turbomole (130, 200, 183, 172, 216, and 200 pm for H, C, N, O, S, and Fe, respectively) [132].

Absolute reduction potentials were estimated from these energies in a solvent according to:

$$E^0 = E(\text{ox}) - E(\text{red}) - 4.43 \qquad (1)$$

where the factor of 4.43 eV represents the potential of the standard hydrogen electrode [133]. The reduction potentials can be compared to those of the $Fe^{II/III}PorIm_2$ (cytochrome) model, calculated with the same method: 0.392, –0.377, and –0.722 V in vacuum, and with $\varepsilon = 4$ and 80, respectively. This is in reasonable agreement with the experimental reduction potentials of His_2 ligated cytochromes *b* and *c*, ranging from –0.4 to +0.5 V [1, 134]. Likewise, we put the proton affinity calculations into a perspective by comparing them to the proton affinity of neutral imidazole (Im), calculated with the same method (–992.5, –1145.69, and –1215.68 kJ/mole in vacuum, and with $\varepsilon = 4$ and 80, respectively).

It important to note that the aim of the present investigation is to compare the *intrinsic* properties of a haem site with different axial ligands. Therefore, we do not want to include

1 Shaik and coworkers have argued that SH^- is a better model of Cys than CH_3S^- [56,64]. However, a recent QM/MM study [45], where a larger reference model for Cys was used ($HCONHCH(CH_2S)CONH_2$), showed that SCH_3^- gives better geometries than does SH^- ($SH^- < SCH_3^- <$ full). SH^- gives better spin densities in vacuum ($SCH_3^- <$ full $< SH^-$), but the opposite is true in the protein. Based on these results and trends, we judge SCH_3^- as a better model than SH^-, in agreement the selection made by most other investigators of cytochrome P450 [e.g. 52,57,73], as well as in almost all other parts of computational biochemistry [120,121].

any atomic detail of a specific protein, which may bias the investigation. Then, it is ideal to model the surrounding protein as a featureless dielectric continuum. However, this will of course make the comparison with experimental data from specific enzymes appreciably harder – in the lack of a detailed atomic model, only qualitative agreement with experimental reduction potentials and proton affinities can be expected.

We also want to point out that for some models, especially compound I (**7**), there are spin states that are nearly degenerate (within 3 kJ/mole). These states have been thoroughly studied and it has been shown that the relative stability of the states is extremely sensitive to the theoretical treatment (model system, method, basis set, model of surroundings, etc.) [14,19,44-62,64,71,77,79-81,85,89,91,108,112,114,115]. Considering the accuracy of state-of-the-art density functional calculations, ~25 kJ/mole [120,121], it is probably impossible to settle with certainty why a certain state is observed in nature. However, since our aim is to compare *geometries* and *energies* of the various models with different axial ligands and these do not change significantly for the various states, the exact state of the models are not important in this investigation (thus, a conspicuous spectroscopic difference does not always imply a significant functional, i.e. energetic, difference). Therefore, we have not attempted to obtain the experimentally observed ground state for all models (even if we normally study both possibilities). The same applies to some models (**5**, **7**, **8**, and **11**), for which the electronic structure seems to be extremely flexible.

Results and Discussion

Spin states

We start the investigation by looking at the relative energies of the various spin states of all models. In this study, we have concentrated on the Cys models, even if we have calculated several spin states also for the other axial ligands. The relative energies of the various spin states are collected in Table 1.

It can be seen that for models **4–6**, **8**, **10–12**, all axial ligands give the same results, viz. an open-shell singlet for the O_2 model **4**, a doublet state for for the reduced O_2 model **5**, the hydroperoxide model **6**, the H_2O_2 model **10**, and the $Fe^{III}OH$ model **12**, and a triplet state for compound II, with or without a proton (**8** and **11**). The other spin states are appreciably less stable (by 14–317 kJ/mole). This is in contrast to the semiempirical calculations of Göller & Clark, which indicated that the two lowest spin states almost degenerate for several of these models, especially **6** [43]. It should be noted that these spin-split energies are hard to calculate and quite uncertain, owing different correlation effects in the various spin states. However, our assignment of the lowest spin state is in accordance with available experimental data [1,2,5,8,9].

For compound I (**7**), all models have nearly degenerate doublet and quartet states (by 0–3 kJ/mole). This degeneracy has been much discussed for the cysteine complex, and the relative energy of the two states is extremely sensitive to the theoretical treatment and the

environment [19,44-62,64,71,77,79-81,85,114,115]. A similar sensitivity has been observed also for compound I in catalase [14] and peroxidase [47,62,80,89,91,108,112]. Our theoretical method is not accurate enough to give the correct ground state for all axial ligands, especially as we do not include a detailed model of the surrounding protein. Therefore, we have studied both states throughout this investigation.

The remaining complexes are of two types: the five-coordinate models (**2** and **3**) and Fe(III) complexes with H_2O or CH_3OH (**1** and **9**). The former complexes are high-spin, for models with negatively charged ligands, even if the intermediate-spin state is close (3 kJ/mole higher) for His+Asp in the Fe(III) state. The other three complexes are most stable in the low-spin state with the negatively charged ligands. However, sometimes the other states are lower in energy (indicated by negative signs in Table 1, e.g. the quartet states with Tyr), but in these complexes, the neutral O-ligand has effectively dissociated from the metal, as is indicated by Fe–O distances longer than 270 pm and by the ligand lying parallel to the haem plane, forming hydrogen bonds to the porphyrin (see below). This is in accordance with the observation of high-spin water–peroxidase complexes with Fe–O distances of 260–270 pm [135] and spectroscopic studies of peroxidases indicating a mixture of five- and six-coordinate states, as well as high- and intermediate-spin states [8].

For the His ligand, on the other hand, the calculations indicate that models **1–3** and **9** are most stable in the intermediate-spin states. This is contrary to experimental observations [66,136,137], and it is a well-known shortcoming of the B3LYP method, giving the wrong spin states of these models [88,99,101,104-107], even if some of them are nearly degenerate. The six-coordinate complexes have weekly bound O-ligands (238–243 pm), but the ligand still interacts with the model by the oxygen atom.

It is notable that a His ligand gives degenerate spin states for the Fe^{II} model, which binds O_2 in the globins, whereas a His+Asp ligands gives degenerate spin states for the Fe^{III} model, which binds H_2O_2 in peroxidase. It has recently been suggested that this degeneracy may accelerate the ligand binding by a factor of ~100 by increasing the probability of the necessary change in spin state during ligand binding (from high- to low-spin) [107,138].

In the following, we will restrict our study to the lowest spin state of each complex, except for compound I (**7**), which we study in both the doublet and quartet states for all ligands, and for the His models of complexes **1–3** and **9,** which we study in both the intermediate-spin state and the spin state that is lowest for the other ligands.

Geometric and electronic structure of the catalase models

Quantum chemical calculations have already been published for all the P450 intermediates [19,43-86] and most of the His intermediates (not **5** and **9**) [47,49,62,66,71,80,81,85,86,88-110]. However, for catalase, only models of compound I or (**7** or **11**) have been studied before [14,80,111,113,114]. Therefore, we will introduce the models by shortly describing the geometric and electronic structures of the phenolate models here. In the following sections,

we will then discuss how the geometry and electronic structure differ in models with the other axial ligands (including those with a Tyr+Arg ligand). The metal–ligand bond lengths and some other geometric parameters of the optimised Tyr complexes are collected in Table 2, and the spin densities are shown in Table 3.

For all tyrosine complexes there exist two possible structures, depending on the relative orientation of the haem and phenolate planes, parallel or perpendicular (cf. Figure 2). In the protein, the parallel conformation is always observed [9]. Therefore, we have concentrated our investigation to this structure. However, for models **3, 5, 7, 8**, and **11**, we have also optimised the perpendicular structure. For all models except **11**, the perpendicular structure is more stable, but the energy difference is not very large (3, 15, 45, 4, 12, and –2 kJ/mole, respectively). Likewise, the two conformations have similar geometric and electronic structures (within 2 pm for the Fe–ligand bond lengths and 0.02 *e* for the spin densities), except for compound I (**7**) and protonated compound II (**8**), for which the flexible spin densities change by up to 0.32 *e*.

Complex **1** ($Fe^{III}H_2O$) is the resting state of cytochrome P450. Figure 3 shows that it is octahedral with an almost planar porphyrin ring (like most of the other tyrosine complexes). The $Fe–O_{Tyr}$ distance is 182 pm and the iron ion is slightly displaced (13 pm) from the porphyrin plane towards this ligand. The water molecule is rather weakly bound to the iron ion (215 pm) and its hydrogen atoms interact with the pyrrole nitrogen atoms, so that the molecule is almost parallel to the porphyrin ring. Most spin density resides on the iron ion (0.98 *e*). However, there is also significant spin density on the phenol ligand, 0.08 *e*, but virtually no spin on water.

If the water molecule is removed (**2**, Fe^{III}), the complex changes from low to high spin. As expected, this change in spin state moves the iron ion distinctly (51 pm) below the porphyrin plane, 184 pm from the phenol ligand. Four of the five unpaired electrons reside on the iron ion, whereas the rest is equally distributed on the phenol ligand and the porphyrin ring. The latter spin density resides mainly on the pyrrole nitrogen atoms (0.10 *e* on each).

When the five-coordinate Fe(III) complex is reduced (**3**), all bonds to the iron ion elongate by 5–10 pm and the iron ion moves even further out of the porphyrin plane (63 pm). The spin density is more concentrated on the iron ion, with only 0.12–0.18 *e* on the phenol ligand and the porphyrin ring.

When the five-coordinate Fe(II) complex binds O_2, there is a spin cross-over again; complex **4** is most stable in the open-shell singlet state, which essentially consists of a low-spin Fe(III) ion, antiferromagnetically coupled to a superoxide radical anion. This is reflected in the spin densities, which show one unpaired electron on the iron ion and one electron on the oxygen molecule (0.42 *e* on the atom bound to iron and 0.62 *e* on the distal oxygen). In this complex, the iron ion moves back into the porphyrin plane. The $Fe–O_{Tyr}$ distance is 193 pm and the other Fe–O distance is 191 pm, i.e. appreciably shorter than for water. The O–O distance is 131 pm, which is slightly shorter than that of free O_2^- (135 pm), calculated with the

same method, but appreciably longer than for free O_2 (121 pm). The Fe–O–O angle is 119º, as expected.

Reduction of this complex leads to only a small elongation of the O–O bond (133 pm). This shows that the electron goes to iron, rather than to the oxygen molecule. This is reflected by a dramatic increase in the Fe–O_{Tyr} distance (to 211 pm) and a more modest increase in the other Fe–O distance (to 195 pm). It is also reflected in the spin densities, which show significant contributions only from the oxygen molecule; only ~0.1 *e* resides on the iron ion and in the porphyrin ring. Thus, model **5** is best characterised as a low-spin $Fe^{II}O_2^-$ complex.

Interestingly, when the oxygen molecule is protonated on the distal oxygen atom (**6**), the electronic structure changes again: The unpaired spin moves from the superoxide ion to the iron ion (0.93 *e)*, forming a $Fe^{III}OH_2^-$ ion pair. The iron ion remains in the porphyrin plane, but the Fe–O distances shorten to 195 and 184 pm, respectively. The O–O distance increases to 146 pm, which is the same as for free H_2O_2, but 6 pm shorter than for free HO_2^-, calculated with the same method. In this vacuum structure, the peroxide hydrogen is directed down towards the porphyrin ring, where it interacts with a pyrrole nitrogen.

The model of compound I (**7**) is most stable in the doublet state, but the quartet state is less than 1 kJ/mole higher in energy. The geometries of the two spin states are almost identical. They have a short Fe–O distance of 162 pm and a very long Fe–O_{Tyr} bond, 235 pm. However, the Fe–N_{Por} distance are not significantly different from those of the other low-spin complexes (~202 pm). The iron ion is 18 pm above the porphyrin plane, towards the oxygen atom. The spin structure is complicated, with ~1.2 *e* on iron, ~0.8 *e* on oxygen, 0.9 *e* on tyrosine, and 0.1–0.2 *e* in the porphyrin ring. Thus, at this level of theory, the system consists approximately of a low-spin Fe(III) ion, a O^- radical, and a neutral tyrosine radical. As Green has pointed out [14], this is not in accordance with experiments, which shows a porphyrin radical instead of the tyrosine radical. He showed that the radical moves if a model of the Arg group that forms two hydrogen bonds to the Tyr ligand in catalase is introduced (a hydrogen bond or even a K^+ ion have the same effect) [14]. He also observed that the tyrosine group rotates as the electronic structure changes. Our results show that the two effects are not correlated: We still obtain the tyrosine radical in the perpendicular orientation if no Arg model is included. Yoshizawa et al. also obtained a ligand radical but a doublet ground state, using a CH_3O^- ligand [114].

If this complex is reduced to compound II (**11**), the electron goes to the tyrosine radical, making it a closed-shell anion again. The spin density of the other groups hardly change: 1.21 *e* on Fe, 0.84 *e* on O, and –0.07 *e* in the porphyrin ring (i.e. essentially $Fe^{III}O^{-\bullet}$). As a consequence, the Fe–O_{Tyr} bond length decreases to 200 pm, whereas the other Fe–O bond length increases slightly to 165 pm.

When compound II is protonated (**8**), the electronic structure changes again. Most of the unpaired electron on the oxygen ligand moves to the iron ion (1.81 *e*), the tyrosine ligand (0.18 *e*), and to the porphyrin ring (–0.15 *e*). Thus, the complex becomes essentially $Fe^{IV}OH^-$,

the only truly high-valent state in this investigation. This leads to a strong elongation of the Fe–O bond (to 180 pm) and a shortening of the Fe–O_{Tyr} bond (to 184 pm). The iron moves into the porphyrin plane, and the ring becomes distinctly saddled (Figure 3).

If this complex is further reduced (**12**), it becomes an almost pure low-spin Fe(III) with a OH^- ligand; the spin density on the OH^-, Tyr, and Por models are all less than 0.1 *e*. This is accompanied with an increase in the two Fe–O distances to 195 (Tyr) and 184 (OH^-) pm.

Finally, the methanol and H_2O_2 complexes (**9** and **10**) are similar to the water complex (**1**), but with a slightly longer Fe–O bond, 219 pm. Interestingly, the H_2O_2 complex has a slightly distorted porphyrin ring. The spin densities indicate almost pure low-spin Fe(III) complex, with essentially no spin on the neutral axial ligand.

In conclusion, we see that the spin states invariably adapt so that the O_2-derived ligand has a single negative charge ($O_2^{-\bullet}$, HO_2^-, $O^{-\bullet}$, or HO^-). The remaining spin ends up on iron (Fe^{II}, Fe^{III}, or Fe^{IV}) or on one of the ligands (axial ligand or porphyrin). We will see below that the electronic structure of models **8**, **11**, and especially **5** and **7** are flexible (they change much with the nature of the ligand or solvation), whereas the other models have stable electronic structures.

Effect of a Tyr+Arg ligand

In all known catalases, the Tyr ligand is hydrogen bonded to the side-chain of a Arg residue [9]. This will partly neutralise the negative charge of the axial ligand, so a realistic model of catalases should include this interaction. Therefore, we have also performed a series of calculations on models where the Arg group has been included as a methylguanidinum ion ($CH_3NHC(NH_2)_2^+$), always in the parallel conformation (see Figure 4). The results are gathered in Tables 4 and 5.

Inclusion of the Arg group leads to a sizeable increase (by 6 pm for the neutral ligands, 2 pm for model **5**, and 9–13 pm for the other models) in the Fe–O_{Tyr} bond length, except for compound I, for which it decreases by 5 (doublet) or 18 pm (quartet state). Therefore, the Fe–O distances decrease, by 7–11 pm for the neutral ligands, but 1–3 pm for the other ligands and a slight increase in compound I. Fe–N_{Por} distances decrease by 2–3 pm in the high-spin states, but hardly at all in the other states.

For most models there is only small differences (up to 0.16 *e*) in the spin densities between the models with and without the Arg model. However, for compound I (**7**), the spin moves partly from the Tyr model to the porphyrin ring (0.51–0.62 *e*), even if 0.42– 0.49 *e* remains on Tyr. The doublet state remains the most stable one, by less than 1 kJ/mole. This is in accordance with the earlier studies by Green [14].

Moreover, the spin state of the reduced O_2 model (**5**) changes even more dramatically. One unpaired spin appears on iron (1.22 *e*) and another in the porphyrin ring (0.91 *e*), whereas without the Arg model, less than 0.12 *e* were found on these moieties. These two spins are then antiferromagnetically coupled to a third spin on O_2 (–1.14 *e*).

Effect of solvation

As mentioned in the introduction, we have also performed wavefunction and geometry optimisations in a continuum solvent, using the COSMO method [128,129]. This gives us the opportunity to study how the geometry and spin distribution changes in solution. Earlier calculations on cytochrome P450 have shown that electronic structure of compound I changes dramatically in solution [45,51]. Thus, we need to examine if this is also the case for Tyr compounds or for the other models. In the tables, we include states for which the geometry changes by more than 5 pm or the spin density by more than 0.1 *e* for any atom or ligand when the structure is reoptimised in a water-like solvent.

From Table 3, it can be seen that the spin state of three Tyr models change significantly. For compounds I and II (**7** and **11**), it is only a redistribution of the spin from O to iron. However, for the reduced O_2 model (**5**), we see a larger change: The spin on iron increases from 0.1 to 0.7 *e*, whereas that on O_2 decreases from 1.0 to 0.4 *e*. Thus, in vacuum, the unpaired electron is located entirely on O_2, whereas in solution it is shared by iron and O_2.

These changes in the electronic state are accompanied by changes in the geometry, as can be seen in Table 2. For all three complexes, the Fe–O_{Tyr} distance decreases, but most for model **5** (by 8 pm). This is accompanied by a slight increase in the other Fe–O distance for models **7** and **11**, whereas that in model **5** decreases by 12 pm. At the same time the O–O distance increases to 142 pm, i.e. closer to that of a peroxide.

For the models with Tyr+Arg (Tables 4 and 5), a similar change in the electronic structure of compound I (**7**) is seen, whereas that of compound II is smaller. For model **5**, the spin state changes back to something similar to the Arg model in vacuum, viz. with 0.25 *e* on iron and 0.85 *e* on O_2.

Influence of the axial ligand on the geometry

In this section we will compare the geometry of the Tyr complexes with that of the complexes with the other axial ligands. The optimised geometries are shown in Figure 6 and the iron–ligand distances are described in Tables 6–8. The replacement of the Tyr ligand with Cys, His, or His+Asp of course leads to changes in the distance between the iron ion and the axial ligand. The three alternative axial ligands all give larger distances to the iron ion than does Tyr: the His+HAsp ligand gives a 5–10 pm longer bond length (13–14 pm for the high-spin complexes **2** and **3**), except for models **5** and **7**, for which the distance actually decreases by 1 and 19 pm, respectively. If the proton is moved to His (HisH+Asp), the Fe–N_{His} bond length increases by 2–3 pm, except for compound I, for which it decreases by 4 pm. Thus, the two His+Asp complexes give axial bond lengths similar to those in the Tyr+Arg complexes. When the Asp group is removed, the Fe–N_{His} bond length increases by another 4–11 pm, once again with models **5** and **7** as exceptions (9 and 1 pm increase). The Cys complexes, with the bulky thiolate ion, give the longest distances to iron, 27–46 pm longer than for tyrosine and

19–45 pm longer than for His.

For almost all complexes, the Fe–O distance is shortest for the His complexes, owing to the long Fe–N_{His} bond and the neutral ligand. Likewise, Tyr+Arg, the other neutral ligand, gives the second shortest Fe–O bonds. The Cys complexes have the longest Fe–O bonds, probably as an effect of a large transfer of charge from S_{Cys} to iron. The Tyr and His+HAsp complexes in general give similar Fe–O bonds, and those in the HisH+Asp complexes are typically ~1 pm shorter. It is notable that the Fe–O bond in compound I is so similar with all axial ligands, 162–164 pm. This is in accordance with EXAFS measurements on various enzymes, all giving the same value, 164±3 pm [11].

Finally, we note that the His and Tyr+Arg complexes give slightly (0.1– 1.7 pm) shorter O–O bonds than the other three axial ligands.

Differences in the electronic structure

In this section, we will continue the comparison of the axial ligand by instead looking at the electronic structure. The spin densities of the various complexes with Cys, His+Asp, and His ligands are shown in Tables 9–11. In general, the Cys complexes have more spin density on the axial ligand than the other complexes, reflecting the softness of the S_{Cys} atom. However, both the His+Asp and Tyr complexes also often have significant spin density on the axial ligand. This is in accordance with the experimental observation of significant spin delocalisation on the axial His ligand in peroxidases [13,108,139,140]. It is also notable that the Cys complexes have the most and the His complexes the least spin density in the porphyrin ring.

For all complexes, except two, there is no qualitative difference in the electronic structure between the various ligands. However, model **5** (the reduced O_2 complex) with a Cys ligand contains 0.76 *e* on iron (i.e. essentially Fe^{III}), antiferromagnetically coupled to 0.70 *e* in the porphyrin ring (in addition to the superoxide radical), i.e. a structure similar to that of the Tyr+Arg model in vacuum. In solution, the density on O_2 and on porphyrin is lower (0.44 and -0.11 e). The other ligands have virtually no spin on iron (i.e. low-spin Fe^{II}) or in the porphyrin ring. We have tried to obtain also the the latter electronic structure for the Cys complex, but with no success.

Second, for compound I (**7**) with a Tyr ligand, we saw that one spin was located on the Tyr ligand (in addition to one unpaired electron on Fe and O, each), but little spin (<0.2 *e*) was found on the porphyrin. However, for His, essentially no spin is found on His (<0.03 *e*). Instead the remaining spin is found on the porphyrin (~1.0 *e*). The same applies also to His+Asp (both protonation states) in water solution. The other ligands have an intermediate spin distribution, with similar spin populations on both the axial ligand and the porphyrin (slightly more on Cys, slightly less on Tyr, when hydrogen-bonded to Arg, and with different trends for the doublet and the quartet for His+HAsp). Finally, the HisH+Asp complex in vacuum differs from the others by having ~0.4 *e* on the *acetate* ligand and ~0.6 *e* on the

porphyrin. In water solution, the spin states of His+Asp changes, whereas for the other complexes, the spin on iron increases slightly, whereas that on O decreases slightly (both by 0.1–0.2 *e*).

This reflects that the electronic structure of compound I is extremely flexible, as has been shown in several investigations [14,19,44-47,49,52,59,62,71,89,91]. Thus, it seems almost meaningless to discuss the spin state of compound I, as it changes with any perturbation in the model system or surrounding. We will see below that these changes have little or no influence on the reaction energies of compound 7. Finally, it should also be noted that in some peroxidases, the radical is actually encountered on a nearby tryptophane residue [89].

Energetics

Finally, we will compare the reaction energies for the intermediates involved in the cytochrome P450, peroxidase, and catalase reaction cycles. The goal of this section is to investigate if there is any difference in the reaction energies of the various axial ligands that may explain the differing reactivity of the various proteins.

The reaction energies of the various reaction steps are collected in Table 12, which contains energies in gas phase and in water solution for the molecules in their ground state. These results should give a feeling of solvation effects in a protein, where the effective dielectric constant is usually assumed to be 2–16 [130,141].

The first reaction in Table 1 (**1** → **2** + H_2O) gives the (negative) binding energy of a water molecule to the five-coordinate Fe(III) complex. The binding is slightly favourable in vacuum (15–28 kJ/mole) for all complexes, except those with Tyr(+Arg). However, solvent effects destabilise the binding and only the His and His+Asp complexes have favourable binding energies in water solution (by 9–16 kJ/mole). This illustrates the weak bonding of the water ligand to the models. We have seen that the picture is complicated by the long Fe–O_{Wat} bond length and the possibility of also high- and intermediate-spin states. However, the results are in accordance with the experimental observation that the resting state of catalase is five-coordinate [9] and that mutations from His to Cys and Tyr ligands in proteins and model systems often lead to a lowered coordination number [26,142].

The second reaction (**2** + e^- → **3**) measures the reduction potential of the five-coordinate Fe(II/III) site. Therefore, this energy is given in V, obtained using Eqn. (1). It can be seen that this potential strongly depends on the total charge of the complex and on solvation effects. In vacuum, it follows the trend Cys < Tyr < His+HAsp < HisH+Asp << Tyr+Arg < His. For the complexes with a (total) negative charge on the axial ligand, the calculated reduction potential is strongly negative and increases in solution (the total charge of the model goes from 0 to –1). The His and Tyr+Arg complexes have an appreciably more positive potential, which decreases in a solvent (owing to the different charge of the models, +1 and 0). In solution,

Tyr+Arg < His+ Asp. This confirms that the axial ligand has a strong effect on the reduction potential, decreasing it if the negative charge is increased, as has been frequently shown experimentally, e.g. by mutagenesis [22-38]. Our results are also in qualitative accordance with the experimental reduction potentials of cytochrome P450 (–0.30 V) [5], horseradish peroxidase (–0.22 V) [8], myoglobin (+0.05 V), catalase (<–0.5 V) [143], except for the lower potential of catalase than cytochrome P450 and that the calculated absolute potentials are too low. However, reduction potentials can easily be tuned by the protein by up to 1 V [144].

The third reaction (**3** + O_2 → **4**) is the binding of O_2 to the reduced haem group. It is exothermic and quite similar (Cys < His+Asp < His < Tyr < Tyr+Arg) for all complexes. The binding energy increases slightly in solution (from 6–37 kJ/mole in vacuum to 38–53 kJ/mole in water). Thus, there is no indication that the haem group in myoglobin should bind O_2 better than the other proteins.

The next reaction (**4** + e^- → **5**) is the reduction of the O_2 complex. Once again, this reduction potential is given in V. It behaves in the same way as the reduction of model **2**, but with appreciable lower potentials, –6.5 to –5.5 V for complexes with a negative ligand (the total charge of the model goes from –2 to –1) and –3.3 V for the His complex in vacuum, and –1.7 to –1.2 in water. As for the other reduction, the order of the reduction potential is Cys < Tyr < His+HAsp < HisH+Asp < Tyr+Arg < His, but in solution, the potential of Tyr+Arg is the lowest one.

The reduction of the O_2 complex increases its proton affinity, which is measured in the next reaction (**5** + H^+ → **6**). To put the proton affinity in a perspective, we assume that the proton comes from an isolated protonated imidazole residue (pK_a = 7.0 [25]). We see that such a proton transfer is highly favourable for the reduced O_2 complex, by 509–824 kJ/mole in vacuum and 52–145 kJ/mole in aqueous solution. The trend is Cys < Tyr < His+HAsp < HisH+Asp < Tyr+Arg His, but once again, the proton affinity of Tyr+Arg is the lowest one in solution. Thus, the His complex has an appreciable lower proton affinity than the other complexes (by 50 kJ/mole = 9 pK_a units in solution). This is a functionally very important difference: The oxygen-binding proteins myoglobin and haemoglobin should bind O_2, but it should not react further (be protonated or reduced), whereas this is the preferred reaction of cytochrome P450. Thus, the higher proton affinity is a manifestation of the push of the negatively charged axial ligands.

We will see below that the reduction potential of model **4** is lower than that of all the other complexes that are reduced in the reaction cycles (**2**, **7**, and **8**) and the proton affinity of model **5** is appreciable larger than of all the other complexes that are protonated (**6**, **11**, and **12**). This probably indicates that the unfavourable reduction is driven by a concerted proton uptake. If

we instead calculate the reduction potential of **4** relative **6**, assuming that the proton comes from a protonated imidazole, the potentials of all axial ligands become similar, positive in vacuum (1.9–2.0 V) and slightly negative in water (–0.6 for His and –0.2 to –0.3 for the other ligands). Thus, the reduction of the O_2 complex is inhibited in the polar site of the globins.

Previous studies of the hydroperoxide complex have shown that a second protonation of the distal oxygen atom leads directly to a water molecule and compound I, without any protonated intermediate [49,53]. Therefore, we have not attempted to find such an intermediate, but we instead study the reaction (**6** + H^+ → **7** + H_2O) as a proton affinity (again comparing with imidazole) coupled with the dissociation of water. It can be seen that the proton affinity of **6** is appreciably lower than that of **5**, –107 (His) to –439 (Cys) kJ/mole in vacuum and –26 (HisH+Asp) to –65 (Tyr) kJ/mole in water. Thus, in vacuum (and at ε = 4), there is a clear push effect of the negative axial ligands (but not of Tyr+Arg), increasing the proton affinity of the hydroperoxide complex and stabilising compound I, but it has disappeared in water solution. This shows that the push effect strongly depends on the effective dielectric constant of the surrounding protein and the nature of the proximal ligand.

In the next step of the cytochrome P450 reaction cycle, compound I reacts with the organic substrate to form an iron-bound alcohol. We have studied both the total reaction (**7** + CH_4 → **9**) and the two proposed reaction steps, hydrogen abstraction from a methyl group (**7** + CH_4 → **8** + $CH_3^{\bullet}$) and radical rebound (**8** + $CH_3^{\bullet}$ → **9**). The hydrogen-atom abstraction is endothermic by a similar amount in all systems (88–107 kJ/mole, Cys < His+Asp < Tyr+Arg < His < Tyr) and with a relatively small solvent effect (~10 kJ/mole). The rebound step is strongly exothermic (–268 to –319 kJ/mole), with a varying solvent effect (–4 to +18 kJ/mole) and an unusual trend: His+Asp < His < Tyr+Arg < Tyr < Cys. The total reaction (**7** + CH_4 → **9**) energy is the sum of these two energies. It is also exothermic by –164 to –230 kJ/mole. Interestingly, it follows the trend His+Asp < His < Tyr+Arg < Cys < Tyr. Thus, the myoglobin model is more effective than the P450 model for this reaction, in accordance with the suggestion that the push effect stabilises the high-valent state and not the product Fe(III) state [36].

The final step in the P450 reaction cycle is the replacement of the alcohol by a water molecule (**9** + H_2O → **1** + CH_3OH). It gives the difference in binding energy of methanol and water to the five-coordinate Fe(III) complex (**2**). The binding of methanol is always favourable (15–89 kJ/mole) and stronger than that of water (by 25–64 kJ/mole, somewhat more in water). Thus, the dissociation of the product is not driven by the thermodynamic force, but rather by the higher concentration of water. The His+Asp complex has the largest difference (i.e. the substitution is 30–50 kJ/mole more unfavourable that for the other

complexes), whereas the other three complexes have similar energies.

We have now studied the full cytochrome P450 reaction cycle and therefore turn to the peroxidase and catalase reactions. We start by studying the binding of H_2O_2 to the five-coordinate Fe(III) complex (**2** + H_2O_2 → **10**), which is the initial step for both peroxidase and catalase. As expected, this reaction is similar to the binding of H_2O to the Fe(III) complex (**2** + H_2O → **1**). Thus, the binding is favourable for all complexes in vacuum, except for those with a Tyr ligand. In water solution, only the His and His+Asp complexes give an exothermic energy. The unfavourable binding of H_2O_2 to the catalase models seems a bit strange. The enzyme probably binds a hydroperoxide anion or enhances the binding of hydrogen peroxide by interactions with the surrounding protein.

The next step in the peroxidase and catalase reaction cycles is the deprotonation of the hydrogen peroxide complex (**10** → **6** + H^+). As usual, this proton affinity is compared to that of imidazole. In vacuum, this reaction is highly unfavourable for complexes with a negatively charged axial ligand, owing to the charge separation. However, in water solution, the reaction becomes slightly exothermic for all complexes (–3 to –56 kJ/mole, with the trend His+Asp < Tyr < His < Cys < Tyr+Arg). In fact, model **6** has the lowest proton affinity of all models investigated (**5**, **6**, **11** and **12**), in accordance with the deprotonation of **10** in the catalase and peroxidase reaction cycles.

We can also study the direct binding of HO_2^- to Fe(III) (**2** + HO_2^- → **6**). It is strongly exothermic in vacuum, with the trend His < Tyr+Arg « HisH+Asp < His+HAsp < Tyr < Cys (–541 to –197 kJ/mole). The stronger binding to the His and Tyr+Arg complexes of course reflects that a negative ligand binds stronger to a positively charged complex than to a neutral one. In water solution, it still exothermic, but by a smaller amount (–101 to –46 kJ/mole).

The following step of peroxidase and catalase, formation of compound I by a second protonation of hydroperoxide (**6** + H^+ → **7** + H_2O), is common to the cytochrome P450 cycle and has already been studied. It is followed in peroxidase by a reduction of compound I by the organic substrate, yielding compound II (**7** + e^- → **11**). As usual, this reduction potential is appreciably lower for the complexes with negatively charged axial ligands than the His and Tyr+Arg complexes, especially in vacuum. However, it is also more negative for Cys (–2.0 V) and Tyr (–1.9 V) than for His+Asp (–1.17). In aqueous solution it is –0.1 to +0.5, with the trend Tyr < Cys < Tyr+Arg = His+Asp < His. The experimental estimate of this reduction potential for horseradish peroxidase is +0.897 V [8], well within the range of the His model, whereas the His+Asp model gives too negative values. The compound I/II reduction potentials with all axial ligands are consistently ~0.9 V more positive than that of the five-coordinate $Fe^{II/III}$ couple, in reasonable agreement with the 1.1-V difference observed

experimentally for horseradish peroxidase [8].

Thus, the selection of the axial ligand may be a way to tune the reduction potentials of compound I and II. That of compound I/II in cytochrome P450 should be as negative as possible to avoid the formation of compound II (as we also observe). This may explain the choice of Cys in cytochrome P450. However, for peroxidase, compound I and II should have similar reduction potentials, because they should both oxidise the same substrate (this is also observed experimentally, e.g. 0.897 and 0.869 V for horseradish peroxidase [8]). Unfortunately, we cannot estimate the reduction potential of the compound II – Fe(III) couple (**11** + e^- + 2 H^+ → **2** + H_2O), because it involves also abstraction of two protons from an unknown source. However, if we assume that they both come from free imidazole, the potential behaves in a similar manner as the other reduction potentials (but with an opposite sign, owing to the opposite total charge of the models), with a high positive potential for the negative ligands (less positive for His and Tyr+Arg), and slightly positive potentials in water (0.0–0.9 V) with the trend Cys ≈ Tyr > Tyr+Arg > His+Asp > His.

However, we can more directly estimate the potential of the **8** + e^- → **12** reaction (protonated compound II to $Fe^{III}OH$ complex). It is consistently 0.1–0.3 V more negative than that of compound I, in accordance with the fact that the two compounds should have similar potentials and even in qualitative agreement with the experimental trend. However, this applies to all ligands, so this is not the reason for the choice of the His+Asp pair in peroxidases.

The proton affinity of compound II (**11** + H^+ → **8**) with negative axial ligands is appreciably higher than for imidazole in vacuum (–467 to –379 kJ/mole), but only slightly higher in aqueous solution (0 to –48 kJ/mole). The neutral His and Tyr+Arg complexes have a lower proton affinity, –94 to –143 kJ/mole in vacuum and +3–32 kJ/mole in water. This is in agreement with EXAFS experiments, which indicate that compound II in CPO is protonated [76]. The same has been suggested to be the case also for peroxidase [20,21,111].

We can also estimate the proton affinity of the $Fe^{III}OH$ complex (12 + H^+ → 1). It is similar to that of compound II, ~10 kJ/mole less negative for the Cys models but ~20 kJ/mole more negative for the other complexes. Thus, it is always higher than that of imidazole, except for the His model in aqueous solution.

Finally, we examine the energetics of the second half reaction of catalase, in which compound I oxidises another molecule of H_2O_2 to O_2 (**7** + H_2O_2 → **2** + H_2O + O_2). This reaction is strongly exothermic for all complexes (–181 to –117 kJ/mole) and relatively insensitive to solvation (~25 kJ/mole less exothermic in aqueous solution). As usual, the His complex is less reactive than the other complexes. In variance to the common trend, the Tyr

complex and especially the Tyr+Arg complex give the most exothermic reaction. Thus, this indicates that a Tyr ligand is actually favourable for the catalase reaction by 8–20 kJ/mole, in accordance with what is found in nature. Looking back, we can see that this effect comes mainly from the unfavourable binding of water to the Tyr complex (**1** → **2** + H_2O).

It has often been suggested that the axial ligand affects the ratio between homolysis and heterolysis of the hydroperoxy complex **6** [e.g. 39]. We can study these two reaction modes by comparing the energies of the two reactions **10** → **7** + H_2O (heterolysis of $Fe^{III}H_2O_2$ to H_2O and compound I) and **10** → **8** + $OH^{\bullet}$ (homolysis of $Fe^{III}H_2O_2$ to $OH^{\bullet}$ and compound II). By this choice of reactions, we avoid the complication of protonations. From the results, it can be seen that the heterolytic reaction is always exothermic, especially in aqueous solution (–66 to –100 kJ/mole). Interesting, the trend is unusual: Tyr(+Arg) < His < Cys < His+Asp. The homolytic reaction is always endothermic (but less so in solution). This is probably an effect of the $OH^{\bullet}$ product and perhaps also that compound II is assumed to be protonated. The trend of the reaction energy is Tyr+Arg < Tyr < Cys < His < His+Asp, but the energies are close (85 to 94 kJ/mole, but 69 kJ/mole for Tyr+Arg) and the trend changes slightly in solution. Therefore, the trend of the *difference* between the hetero- and homolytic reaction energies follows mainly that of the heterolytic reaction: Tyr < His < Tyr+Arg < His+Asp < Cys. Thus, there is no indication that the negative ligands should enhance the heterolytic reaction. On the contrary, Cys shows the smallest difference between the two reactions.

Conclusions

In this article, we have made a systematic investigation of the influence of the axial ligand on the spin-state energies, the geometry, the electronic structure, and the reaction energies of all intermediates involved in the cytochrome P450, peroxidase, and catalase reaction cycles. By using theoretical calculations, we get pure results about the intrinsic differences between the axial ligands, which are not biased by differences in the surrounding protein or the possibility of conformational changes in mutation studies, for example. On the other hand, the quantum chemical energies are enthalpies, rather than the free energies that govern the real chemistry, even if the solvation models estimate the free energy of solvation of the active-site models. This has to be remembered when comparing the results to experiments. We have obtained a considerable amount of data that has been described in a systematic way in the previous sections. In this section, we will pinpoint the most significant differences and discuss them in relation to previous suggestion of the influence of the axial ligands.

The most clear difference between the various axial ligands is seen for the reduction potentials. Thus, the negatively charged Cys and Tyr ligands always give the lowest potentials, whereas the neutral His ligand always give appreciably more positive potentials (by ~0.6 V in water). This is in accordance with mutant studies [22-38]. The potentials with

the His+Asp and Tyr+Arg ligands are intermediate, highest for HisH+Asp and lowest for Tyr+Arg. This is also in accordance with the experimental observation that hydrogen bonds to negatively charged axial ligands tend to increase the reduction potential [30,36,40].

Moreover, this may be the explanation why cytochromes P450 employ a Cys ligand: The reduction potential of compound I/II (**7** → **11**) is 0.4 V more negative for Cys than for His+Asp. Thus, it is easier to reduce compound I with a His+Asp ligand, which is in accordance with the one-electron chemistry of peroxidases, whereas it is harder with the Cys ligand, in accordance with the hydroxylation reaction of cytochrome P450.

A second important difference is found for the reduction potential and proton affinity of the O_2 complexes (**4** and **5**): The His models have appreciably lower potentials and proton affinities than the other axial ligands, even in water solution. This should have great functional importance, prohibiting the formation of the hydroperoxy intermediate in the globins, which could lead to the formation of harmful reactive oxygen species. Likewise, it would be undesirable if the hydroperoxide complex (**6**) could be deprotonated or oxidised for the peroxidases, catalases, or cytochrome P450. Therefore, the choice a neutral His ligand in the globins, and a negatively charged ligand for the other enzymes seems to be well motivated by these reactions.

Thus, the results in general show a distinct difference between His and the negatively charged ligands (Cys, Tyr, and His+Asp). The difference is most pronounced in vacuum (where Tyr+Arg is similar to His) and for the reduction potentials and proton affinities, where the total charge of the model mainly determines the energetics. Moreover, the same distinction exists for the spin energies, where the negative ligands have the same ground states for all complexes (except the degenerate compound I), whereas several His complexes show differing ground states. In water solution, the energetic differences are smaller, but still most reactions show the general trend Cys < Tyr < Tyr+Arg < His+Asp < His, illustrating the change in the donor capacity of the ligand.

However, for the binding of neutral ligands, instead the Tyr(+Arg) complexes fall out by giving the lowest binding energies. This seems to slightly favour the second catalase half reaction (**1** → **2** + H_2O) of the Tyr+Arg complex compared to the other axial ligands, and it may be the explanation why these ligands were used in catalase.

Thus, the present results confirm the common view [3,117] that the axial ligand has a clear effect on reduction potentials (a negatively charged ligand stabilises the oxidised forms), including the high-valent compound I. However, our results do *not* support several other proposals. For example, they do not support the suggestion that a negatively charged axial ligand should inhibit reprotonation of the hydroperoxide complex (leading to the formation the H_2O_2 complex **10**) [36]. On the contrary, the His model of complex **6** has an appreciably

lower proton affinity than the negatively charged ligands in vacuum and an intermediate affinity in water solution.

Earlier theoretical studies have found an important effect of the axial ligand on the formation of compound I (**6** → **7**) [49]. We also observe this effect in vacuum, illustrating that it is mainly caused by the charge of the ligand. However, our results show that the effect depends strongly on the surroundings of the haem group. Thus, in aqueous solution, the effect has disappeared; instead the trend is Tyr < Cys < His < Tyr+Arg < His+Asp, where the three first differ by only 4 kJ/mole. Therefore, we cannot draw any conclusive inferences for this reaction without a detailed study of the active sites in the various proteins.

It has also frequently been suggested that a negative axial ligand influences whether the hydroperoxide complex reacts by heterolysis or homolysis, with a thiolate favouring heterolysis [24,26,33-35]. Once again, our reaction energies do not confirm such a suggestion. On the contrary, we find the trend Tyr < His < Tyr+Arg < His+Asp < Cys, both in vacuum and water, for the difference between the heterolytic and homolytic reaction energy. Thus, this effect probably comes from the reaction barriers, rather than from the reaction energies [47,81].

In conclusion, we have seen that theoretical calculations can provide interesting information about the intrinsic influence of the axial ligand on the properties of the haem proteins in a pure and unbiased way. In particular, we can explain the distinction between a neutral His ligand and the other axial ligands, and we have also seen indications why Tyr is used in catalases and why Cys is used in cytochromes P450. For further clues about the choice of the axial ligand, we need to study activation energies and the detailed structure of the various proteins.

Acknowledgements

This investigation has been supported by funding from the Research School in Medicinal Chemistry (FLÄK) at Lund University and from the Swedish research council. It has also been supported by computer resources of the Swedish Council for Planning and Coordination of Research (FRN), Parallelldatorcentrum (PDC) at the Royal Institute of Technology, Stockholm, the High Performance Computing Centre North (HPC2N) at the University of Umeå, and Lunarc at Lund University.

References

1. Fraústo da Silvia JJR, Williams PJ (1994) The biological chemistry of the elements. Claredon Press, Oxford
2. Kaim W, Schwederski B (1996) Bioinorganic chemistry: inorganic elements in the chemistry of life. John Wiley & Sons, Chichester
3. Poulos TL (1996) J Biol Inorg Chem 1:356-359
4. Sigfridsson E, Olsson MHM, Ryde U (2001) J Phys Chem B 105:5546-5552
5. Li H (2001) In: Messerschmidt A, Huber R, Poulos T, Wieghart K (eds) Handbook of Metalloproteins. J. Wiley & Sons, Chichester, pp 486-502
6. Sundaramoorthy M (2001) In: Messerschmidt A, Huber R, Poulos T, Wieghart K (eds) Handbook of Metalloproteins. J. Wiley & Sons, Chichester, pp 233
7. Rosenfeld (2001) In: Messerschmidt A, Huber R, Poulos T, Wieghart K (eds) Handbook of Metalloproteins. J. Wiley & Sons, Chichester, pp 285
8. Gajhede M (2001) In: Messerschmidt A, Huber R, Poulos T, Wieghart K (eds) Handbook of Metalloproteins. J. Wiley & Sons, Chichester, pp 195-209
9. Maté MJ, Bravo J, Fita I, Murshudov G, Melik-Adamyan W, Loewen PC (2001) In: Messerschmidt A, Huber R, Poulos T, Wieghart K (eds) Handbook of Metalloproteins. J. Wiley & Sons, Chichester, pp 486-502
10. Goodin J (1996) Biol Inorg Chem 1:360-363
11. Gross Z (1996) Biol Inorg Chem 1:368-371
12. Rietjens IMCM, Osman AM, Veeger C, Zakharieva O, Antony J, Grodzicki M, Trautwein AX (1996) Biol Inorg Chem 1:372-376
13. Weiss J, Mandon D, Wolter T, Trautwein AX, Müther M, Bill E, Gold A, Jayaraj K, Terner J (1996) Biol Inorg Chem 1:377-383
14. Green MT (2001) J Am Chem Soc 123:9218-9219
15. Poulos TL (1995) Curr Opin Struct Biol 5:767-774
16. Sono M, Roach MP, Coulter ED, Dawson JH (1996) Chem Rev 96:2841-2887
17. Ohno J, Suzuki N, Dokoh T, Urano Y, Kikuchi K, Hirobe M, Higuchi T, Nagano T (2000) Inorg Biochem 82:123-125
18. Schlichting, Berendzen J, Chu K, Stock AM, Maves SA, Benson DE, Sweet RM, Ringe D, Petsko GA, Sligar SG (2000) Science 287:1615-1622
19. Shaik S, de Visser SP, Ogliaro F, Schwarz H, Schröder D (2002) Curr Opin Chem Biol 6:556-557
20. Hersleth HP, Dalhus B, Goerbitz CH (2002) J Biol Inorg Chem 7:299-304
21. Berglund GI, Hajdu J (2002) Nature 417:463-468
22. Hildebrand DP, Ferrer JC, Tang HL, Smith M, Mauk AG (1995) Biochemistry 34:11598-11605
23. Hildebrand DP, Burk DL, Maurus R, Ferrer JC, Brayer GD, Mauk AG (1995) Biochemistry 34:1997-2005
24. Adachi S, Nagano S, Ishimori K, Watanabe Y, Morishima I, Egawa T, Kitagawa T, Makino R (1993) Biochemistry 32:241-252
25. Roach MP, Ozaki S, Watanabe Y (2000) Biochemistry 39:1446-1454
26. Liu Y. Moënne-Loccoz P, Hildebrand D, Wilks A, Loehr TM, Mauk AG, Ortiz de Montellano PR (1999) Biochemistry 38:3733-3743
27. Choudhury K, Sundaramoorthy M, Hickman A, Yonetani T, Woehl E, Dunn MF, Poulos TL (1994) J Biol Chem 269:20239-20249
28. Sigman JA, Pond AE, Dawson JH, Lu Y (1999) Biochemistry 38:11122-11129
29. Hirst J, Wilcox SK, Jingyuan A, Moënne-Loccoz P, Loehr TM, Goodin DB (2001) Biochemistry 40:1274-1283
30. Erman JE, Vitello LB (2002) Biochim Biophys Acta 1597:193-220
31. McRee DE, Jensen GM, Fitzgerald MM, Siegel HA, Goodin DB (1994) Proc Natl Acad Sci USA 91:12847-12851
32. Shimizu T, Hirano K, Takahashi M, Hatano M, Fujii-Kuriyama Y (1988) Biochemistry 27:4138-4141
33. Auclair K, Moenne-Loccoz P, de Montellano O (2001) J Am Chem Soc 123:4877-4885
34. Vatsis KP, Peng HM, Coon MJ (2002) J Inorg Biochem 91: 542-553

35. Yoshioka S, Takahashi S, Hori H, Ishimori K, Morishima I (2001) Eur J Biochem 268:252-259
36. Yoshioka S, Takahashi S, Ishimori K, Morishima I (2000) J Inorg Biochem 81:141-151
37. Yi X Mroczko M, Manoj KM, Wang X, Hager LP (1999) Proc Natl Acad Sci USA 96:12412-12417
38. Raphael AL, Gray HB (1991) J Am Chem Soc 113:1038-1040
39. Higuchi T, Shimada K, Maruyama N, Hirobe M (1993) J Am Chem Soc 115:7551-7552
40. Suzuki N, Higuchi T, Urano Y, Kikuchi K, Uekusa H, Ohashi Y, Uchida T, Kitagawa T, Nagano T (1999) J Am Chem Soc 121:11571-11572
41. Higuchi T, Uzu S, Hirobe M (1990) J Am Chem Soc 112:7051-7053
42. Traylor TG, Popovitz-Biro R (1988) J Am Chem Soc 110:239-243
43. Göller AH, Clark T (2001) J Mol Struct Theochem 541:263-281
44. Harris DL (2001) Curr Opin Chem Biol 5:724-735
45. Schöneboom JC, Lin H, Reuter N, Thiel W, Cohen S, Ogliaro F, Shaik S (2002) J Am Chem Soc 124:8142-8151
46. Ogliaro F, de Visser SP, Cohen S, Sharma PK, Shaik S (2002) J Am Chem Soc 124:2806-2817
47. Harris DL, Loew GH (2001) J Porph Phtalacy 5:334-344
48. Ogliaro F, de Visser SP, Cohen S, Kaneti J, Shaik S (2001) ChemBioChem 11:848-851
49. Ogliaro F, de Visser SP, Shaik S (2002) J Inorg Biochem 91:554-567
50. Harris DL, Loew G, Waskell L (2001) J Inorg Biochem 83:309-318
51. Ogliaro F, Cohen S, de Visser SP, Shaik S (2000) J Am Chem Soc 122:12892-12893
52. Green MT (1999) J Am Chem Soc 121:7939-7940
53. Harris DL, Loew GH (1998) J Am Chem Soc 120:8941-8948
54. Yoshizawa K, Kagawa Y, Shiota Y (2000) J Phys Chem B 104:12365-12370
55. de Visser SP, Ogliaro F, Harris DL, Shaik S (2001) J Am Chem Soc 123:3037-3047
56. Ogliaro F, Harris N, Cohen S, Filatov M, de Visser SP, Shaik S (2000) J Am Chem Soc 122:8977-8989
57. Yoshizawa K, Ohta T, Eda M, Yamabe T (2000) Bull Chem Soc Jpn 73:401-407
58. Yoshizawa K, Shiota Y, Kagawa Y (2000) Bull Chem Soc Jpn 73:2669-2673
59. de Visser SP, Ogliaro F, Sharma PK, Shaik S (2002) J Am Chem Soc 124:11809-11826
60. Ogliaro F, Filatov M, Shaik S (2000) Eur J Inorg Chem 2455-2458
61. Yoshizawa K, Kamachi T, Shiota T (2001) J Am Chem Soc 123:9806-9816
62. Green MT (2000) J Am Chem Soc 122:9495-9499
63. Murphy RB, Philipp DM, Friesner RA (2000) J Comp Chem 21:1442-1457
64. Ogliaro F, Cohen S, Filatov M, Harris N, Shaik S (2000) Angew Chem Int Ed 39:3851-3855
65. Filatov M, Harris N, Shaik S (1999) Angew Chem Int Ed 38:3510-3512
66. Green MT (1998) J Am Chem Soc 120:10772-10773
67. de Groot MJ, Havenith RWA, Vinkers HM, Zwaans R, Vermeulen NPE, van Lenthe JH (1998) J Comp Aid Mol Des 12:183-193
68. Harris DL, Loew GH, Waskell L (1998) J Am Chem Soc 120:4308-4318
69. Segall MD, Payne MC, Ellis SW, Tucker GT, Boyes RN (1998) Xenobiotica 28:15-20
70. Segall MD, Payne MC, Ellis SW, Tucker GT, Boyes RN (1998) Phys Rev E 57:4618-4621
71. Antony J, Grodzicki M, Trautwein AX (1997) J Phys Chem A 101:2692-2701
72. Harris DL, Loew GH (1996) J Am Chem Soc 118:10588-10594
73. Loew GH, Harris DL (2000) Chem Rev 100:407-419
74. Harris DL, Loew GH (1993) J Am Chem Soc 115:5799-5802
75. Guallar V, Harris DL, Batista VS, Miller WH (2002) J Am Chem Soc 124:1430-1437
76. Green M.T, Gray H.B (2002) Abstracts of the 6th European conference on biological inorganic chemistry, Lund, pp. 255
77. Guallar V, Gherman BF, Lippard SJ, Friesner RA (2002) Curr Opin Chem Biol 6:236-242

78. Segall MD, Payne MC, Ellis SW, Tucker GT, Eddershaw PJ (1999) Xenobiotica 29:561-571
79. Loew GH (2000) Int J Quantum Chem 77:54-70
80. Du P, Loew GH (1992) Int J Quantum Chem 44:251-261
81. Zakharieva O, Grodricki M, Trautwein AX, Veeger C, Rietjens IMCM (1996) J Biol Inorg Chem 1:192-204
82. Harris DL (2002) J Inorg Biochem 91:568-585
83. Harris N, Cohen S, Filatov M, Ogliaro F, Shaik S (2000) Angew Chem Int Ed 39:2003-2007
84. Harris DL, Loew GH (1993) J Am Chem Soc 115:8775-8779
85. Loew GH, Kert CJ, Hjelmeland LM, Kirchne RF (1977) J Am Chem Soc 99:3534-3536
86. Rohmer M-M, Dedieu A, Veillard A (1983) Chem Phys 77:449-462
87. Guallar V, Baik M-H, Lippard SJ, Friesner RA (2003) Proc Natnl Ac Sci US 100:6998-7002
88. Maréchal J.D, Maseras F, Lledós A, Mouawad L, Perahia D (2002) Chem Phys Lett 353:379-382
89. Wirstam M, Blomberg MRA, Siegbahn PEM (1999) J Am Chem Soc 121:10178-10185
90. Vangberg T, Ghosh A (1999) J Am Chem Soc 121:12154-12160
91. Deeth RJ (1999) J Am Chem Soc 121:6074-6075
92. Kuramochi H, Noodleman L, Case DA (1997) J Am Chem Soc 119:11442-11451
93. Loew GH, Depuis M (1996) J Am Chem Soc 118:10584-10587
94. Loew GH, Depuis M (1997) J Am Chem Soc 119:9848-9851
95. Rovira C, Parrinello M (2000) Biophys J 78:93-100
96. Rovira C, Parrinello M (2000) Int J Quantum Chem 80:1172-1180
97. Rovira C, Parrinello M (1999) Chem Eur J 5:250-262
98. Rovira C, Kunc K, Hutter J, Ballone P, Parrinello M (1998) Int J Quantum Chem 69:31-35
99. Rovira C, Kunc K, Hutter P, Ballone P, Parrinello M (1997) J Phys Chem A 101:8914-8925
100. Bytheway I, Hall MB (1994) Chem Rev 94:639-658
101. Marechal JD, Barea G, Maseras F, Lledós A, Mouawad L, Pérahia D (2000) J Comput Chem 21:282-294
102. Vogel KM, Kozlowski PM, Zgierski MZ, Spiro TG (1999) J Am Chem Soc 121:9915-9921
103. Spiro T.G, Zgierski M.Z, Kozlowski P.M (2001) Coord Chem Rev 219-221:923-936
104. Sigfridsson E, Ryde U (1999) J Biol Inorg Chem 4:99-110
105. Sigfridsson E, Ryde U (2002) J Inorg Biochem 91:116-124
106. Jensen KP, Ryde U (2003) ChemBioChem 4:413-424
107. Jensen KP, Ryde U (2003) Mol Phys 101:2003-2018
108. Loew GH, Axe FU, Collins JR, Du P (1991) Inorg Chem 30:2291-2294
109. Loew GH, Herman ZS (1980) J Am Chem Soc 102:6173-6174
110. Karle Hanson L, Chang CK, Davis MS, Fajer J (1981) J Am Chem Soc 103:663-670
111. Rovira C, Fita I (2003) J Phys Chem B 107:5300-5305
112. Menyhárd D.K, Náray-Szabó G (1999) J Phys Chem B 103:227-233
113. Du P, Loew G.H (1995) Biophys J 68:69-80
114. Ohta T, Matsuura K, Yoshizawa K, Morishima I (2000) J Inorg Biochem 82:141-152
115. Filatov M, Harris N, Shaik S (1999) J Chem Soc Perkin Trans 2 3:399-410
116. Poulos TL (1987) Adv Inorg Biochem 7:1-36
117. Dawson JH (1998) Science 240:433-439
118. Treutler D, Ahlrichs R (1995) J Chem Phys 102:346-354
119. Hertwig R., Koch W (1997) Chem Phys Lett 268:345-351
120. Siegbahn PEM, Blomberg MRA (1999) Annu Rev Phys Chem 50:221–249
121. Siegbahn PEM, Blomberg MRA (2000) Chem Rev 100:421–437
122. Bauschlicher CW (1995) Chem Phys Lett 246:40-44
123. Schäfer A, Horn H, Alrichs R (1992) J Chem Phys 97:2571-2577
124. Hehre WJ, Radom L, Schleyer PvR, Pople JA (1986) Ab initio molecular orbital theory. Wiley-Interscience, New York

125. Ryde U, Olsson MHM, Roos BO, Borin-Carlos A (2001) Theor Chem Acc 105:452-462
126. Sigfridsson E, Ryde U (2003) J Biol Inorg Chem 8:273-282
127. Guallar V, Baik MH, Lippard SJ, Friesner RA (2003) Proc Natl Acad Sci US 100:6998-7002
128. Klamt A, Schüürmann J (1993) J Chem Soc Perkin Trans 2 5:799-805
129. Schäfer A, Klamt A, Sattel D, Lohrenz JCW, Eckert F (2000) Phys Chem Chem Phys 2:2187-2193
130. Sharp KA, Honig B (1990) Annu Rev Biophys Biophys Chem 19:301-332
131. Honig B, Nicholls A (1995) Science 268:1144-1149
132. Klamt A, Jonas V, Bürger T, Lohrenz JCW (1998) J Phys Chem 102:5074-5085
133. Reiss H, Heller A (1985) J Phys Chem 89:4207-4213
134. Zhou H-X (1997) J Biol Inorg Chem 2:109-113
135. Smulevich G, Feis A, Indiani C, Becucci M, Marzocchi MP (1999) J Biol Inorg Chem 4:39-47
136. Seibold S, Cerda JF, Mulichak AM, Song I, Garavito M, Arakawa T, Smith WL, Babcock GT (2000) Biochemistry 39:6616-6624
137. Sun J, Wilks A, Ortiz de Montellano PR (1993) Biochemistry 32:14151-14157
138. Jensen KP, Ryde U (2004), Chem Eur J, submitted
139. Oertling WA, Babcock GT (1988) Biochemistry 27:3331-3338
140. Thanabal V, La Mar GN, de Ropp JS (1988) Biochemistry 27:5400-5407
141. Sharp KA, Honig B (1990) Annu Rev Biophys Biophys Chem 19:301-302
142. Roach MP, Pond AE, Thomas MR, Boxer SG, Dawson JG (1999) J Am Chem Soc 121:12088-12093
143. Adachi S, Nagano S, Watanabe Y, Ishimori K, Morishima I (1991) Biochem Biophys Res Commun 180:138-144
144. Stephens PJ, Jollie DR, Warshel A (1996) Chem Rev 96:2491-2513

Table 1. Spin-splitting energies of complexes with the various axial ligands. Values in parenthesis for some singlet states indicate open-shell singlets.

Complex	Spin state	Relative Energy (kJ/mole)			
		Cys	Tyr	His+Asp	His
1	2	0.0	0.0	0.0	11.6
$Fe^{III}H_2O$	4	56.2	–7.7	18.3	**0.0**
	6	–1.5	–28.5	13.3	27.7
2	2	9.8	47.8	13.2	42.3
Fe^{III}	4	50.3	13.9	3.4	**0.0**
	6	0.0	0.0	0.0	23.5
3	1	47.2			30.1
Fe^{II}	3	31.6	41.7	16.2	**0.0**
	5	0.0	0.0	0.0	1.9
4	1	76.0	74.2	70.3	74.2
$Fe^{III}O_2^-$	Open-shell 1	0.0	0.0	0.0	0.0
	3	13.5			
	5	60.55			
5	2	0.0	0.0	0.0	0.0
$Fe^{II}O_2^-$	4	20.7	45.1	48.3 (59.0)	45.1
	6		15.5		
6	2	0.0	0.0	0.0	0.0
$Fe^{III}HO_2^-$	4	140.5	50.9	63.6	50.9
	6	317.4			
7	2	–0.9	–0.3, –0.2[a], –0.2[b]	0.3, –3.4[c]	0.4
compound I	4	0.0	0.0	0.0	0.0
	6	48.7		50.8	49.2
8	1	17.4	11.6		47.9 (24.2)
$Fe^{IV}OH^-$	3	0.0	0.0	0.0	0.0
	5	20.8			101.2
	7				146.3
9	2	0.0	0.0	0.0	9.8
$Fe^{III}CH_3OH$	4	50.1	–11.6	17.1	**0**
	6	0.5			
10	2	0.0	0.0	0.0	0.0
$Fe^{III}H_2O_2$	4	49.9	–14.3		18.1
	6	2.7			
11	1	122.8			116.6 (32.0)
compound II	3	0.0	0.0	0.0	0.0
	5	124.8			90.5
	7				248.7
12	2	0.0	0.0	0.0	0.0
$Fe^{III}OH^-$	4	54.5			106.2
	6	46.4			75.6

[a] With an Arg model.
[b] The perpendicular conformational.
[c] The HisH+Asp conformation.

Table 2. Geometries of the various models with an axial Tyr ligand. "Perpend." means that the phenol ring is perpendicular (rather than parallel) to the porphyrin ring, cf. Figure 2.

Model	spin state	Fe–O_{Tyr}	Fe–N_{Por}	Fe–$N_{Por,av}$	Fe–O	O–O	O–H	Fe–O–O	Fe outp
1 – $Fe^{III}H_2O$	2	182.3	200.7–203.5	202.1	215.3		97.5		–12.8
	4	189.5	201.9–203.2	202.6	276.3		97.0		–25.1
	6	182.9	209.9–211.3	210.6	370.9		97.1		–52.8
2 – Fe^{III}	6	183.5	210.2–210.5	210.3					–51.0
3 – Fe^{II}	5	194.2	215.6–215.8	215.7					–62.6
	perpend.	194.8	215.6–216.0	215.8					–63.1
4 – $Fe^{III}O_2^-$	os 1	192.9	201.4–203.5	202.4	190.8	130.6		119.2	–2.6
5 – $Fe^{II}O_2^{2-}$	2	210.8	201.2–202.9	202.0	193.8	133.0		120.3	0.9
	ε = 80	202.7	200.9–203.7	202.3	182.0	142.0		120.7	2.9
	perpend.	211.1	201.3–202.7	202.1	194.6	133.0		120.6	0.4
6 – $Fe^{III}OOH^-$	2	194.9	201.3–203.6	202.6	184.4	145.8	97.2	116.4	0.5
7 – Compound I	2	235.4	201.4–202.0	201.8	161.6				17.9
	ε = 80	228.8	201.5–201.8	201.6	162.7				17.0
	perpend.	229.2	201.7–202.3	202.0	161.7				15.8
	4	235.0	201.6–201.9	201.8	161.7				17.6
	ε = 80	236.9	201.3–201.6	201.5	162.6				19.0
	perpend.	235.1	201.8–202.0	201.9	161.6				17.0
8 – $Fe^{IV}OH^-$	3	183.5	200.7–202.5	201.8	180.0		97.4		–1.0
	perpend.	185.3	200.6–202.5	201.5	179.4		97.3		–1.3
9 – $Fe^{III}CH_3OH$	2	182.9	201.4–202.3	201.9	218.5		97.3		–12.1
	4	190.2	202.1–203.3	202.5	274.7		97.1		–24.2
10 – $Fe^{III}H_2O_2$	2	182.1	200.3–203.4	202.0	218.8	145.5	98.6	116.3	–14.2
							97.8		
			201.8–203.8				98.2		–28.1
	4	188.6		202.7	293.5	145.5	97.5	104.4	
11 – $Fe^{III}O^-$	3	200.3	202.5–203.1	202.8	164.9				7.4
	ε = 80	199.2	202.1–202.9	202.5	165.9				8.0
	perpend.	200.3	202.5–203.1	202.8	164.7				6.3
12 – $Fe^{III}OH^-$	2	194.7	202.1–203.2	202.7	183.9		97.2		0.4

Table 3. Spin densities of the various models with an axial Tyr ligand. "Perpend." means that the phenol ring is perpendicular (rather than parallel) to the porphyrin ring, cf. Figure 2,

	Spin state	Fe	O_{Tyr}	O	$N_{Por,av}$	Tyr	O–ligand	Porf
1 – $Fe^{III}H_2O$	2	0.978	0.086	–0.003	–0.016	0.077	–0.003	–0.052
2 – Fe^{III}	6	4.129	0.307		0.099	0.394		0.477
3 – Fe^{II}	5	3.695	0.087		0.031	0.120		0.185
	perpend.	3.700	0.086		0.031	0.116		0.184
4 – $Fe^{III}O_2^-$	os1	1.056	0.065	–0.423 –0.622	–0.020	0.065	–1.045	–0.076
5 – $Fe^{II}O_2^{2-}$	2	0.110	0.001	0.450 0.518	0.002	–0.001	0.968	–0.077
	ε = 80	0.705	0.016	0.248 0.129	–0.007	0.015	0.377	–0.096
	perpend.	0.094	–0.001	0.450 0.521	0.003	–0.001	0.971	–0.064
6 – $Fe^{III}OOH^-$	2	0.932	0.045	0.093 –0.001	–0.015	0.044	0.094	–0.070
7 – Compound I	2	1.247	–0.351	0.817	–0.030	–0.867	0.816	–0.198
	ε = 80	1.373	–0.364	0.700	–0.014	–0.990	0.700	–0.083
	perpend.	1.214	–0.408	0.846	–0.006	–0.991	0.846	–0.069
	4	1.208	0.348	0.837	0.019	0.866	0.837	0.089
	ε = 80	1.369	0.333	0.696	0.000	0.930	0.696	0.005
	perpend.	1.215	0.393	0.833	–0.002	0.986	0.833	–0.035
8 – $Fe^{IV}OH^-$	3	1.810	0.170	0.151	–0.040	0.182	0.157	–0.149
	perpend.	1.490	0.276	0.137	–0.028	0.492	0.137	–0.119
9 – $Fe^{III}CH_3OH$	2	0.993	0.075	–0.006	–0.017	0.064	–0.005	–0.062
10 – $Fe^{III}H_2O_2$	2	0.987	0.081	–0.005 0.001	–0.016	0.068	–0.003	–0.052
11 – $Fe^{III}O^-$	3	1.217	0.029	0.842	–0.008	0.029	0.842	–0.088
	ε = 80	1.382	0.030	0.692	–0.016	0.029	0.692	-0.103
	perpend.	1.206	0.025	0.844	–0.008	0.038	0.844	–0.088
12 – $Fe^{III}OH^-$	2	0.929	0.052	0.097	–0.015	0.051	0.093	–0.073

Table 4. Geometries of the various models with an Tyr+Arg ligand.

Model	spin state	Fe–O_{Tyr}	Fe–N_{Por}	Fe–$N_{Por,av}$	Fe–O	O–O	O–H	Fe–O–O	Fe outp
1 – $Fe^{III}H_2O$	2	188.2	200.1–203.3	201.7	207.7		97.5		–10.3
2 – Fe^{III}	6	193.2	207.3–210.0	208.6					–45.8
3 – Fe^{II}	5	205.0	211.2–214.6	212.9					–51.8
4 – $Fe^{III}O_2^-$	os 1	206.3	200.4–203.5	202.0	188.9	129.1		118.9	–1.0
5 – $Fe^{II}O_2^{2-}$	2	212.7	200.7–205.8	203.0	189.0	129.3		119.5	0.4
6 – $Fe^{III}OOH^-$	2	206.0	200.3–204.1	202.3	181.3	144.7	97.5	115.9	2.1
7 – Compound I	2	230.0	201.1–202.6	201.9	162.0				13.3
	4	217.5	201.1–202.8	202.0	162.2				11.9
8 – $Fe^{IV}OH^-$	3	194.2	200.2–203.1	201.2	177.7		97.5		–2.3
9 – $Fe^{III}CH_3OH$	2	188.7	200.1–203.6	201.7	207.4		97.3		–8.6
10 – $Fe^{III}H_2O_2$	2		200.6–202.2				98.2		–11.7
		187.7		201.6	211.4	146.1	97.7	116.2	
11 – $Fe^{III}O^-$	3	216.2	201.5–203.3	202.0	163.0				10.2
12 – $Fe^{III}OH^-$	2	205.8	201.6–203.3	202.4	180.9		97.3		2.5

Table 5. Spin densities of the various models with an axial Tyr+Arg ligand.

	Spin state	Fe	O_{Tyr}	O	$N_{Por,av}$	Tyr	O–ligand	Porf
1 – $Fe^{III}H_2O$	2	1.033	0.029	–0.005	–0.021	0.020	–0.004	–0.052
2 – Fe^{III}	6	4.180	0.197		0.112	0.244		0.574
3 – Fe^{II}	5	3.729	0.055		0.031	0.073		0.199
4 – $Fe^{III}O_2^-$	os1			–0.675	–0.024		–1.142	–0.079
		1.201	0.017	–0.467		0.019		
5 – $Fe^{II}O_2^{2-}$	2			–0.485			–1.145	
		1.218	0.009	–0.660	0.015	0.011		0.912
	ε = 80			0.433				–0.097
		0.251	0.000	0.414	0.003	0.000	0.847	
6 – $Fe^{III}OOH^-$	2			0.091	–0.016			–0.063
		0.967	0.011	–0.008		0.009	0.086	
7 – Compound I	2	1.230	–0.186	0.869	–0.084	–0.481	0.869	–0.615
	ε = 80	1.388	–0.209	0.734	–0.083	–0.539	0.734	-0.578
	4	1.132	0.164	0.893	0.084	0.424	0.893	0.547
	ε = 80	1.256	0.121	0.779	0.094	0.276	0.779	0.687
8 – $Fe^{IV}OH^-$		1.929	0.035	0.172	0.043	0.023	0.178	–0.134
	3					0.005		
9 – $Fe^{III}CH_3OH$	2	1.035	0.026	–0.002	–0.021	0.016	–0.001	–0.052
10 – $Fe^{III}H_2O_2$	2	1.035		–0.002	–0.020	0.017	–0.007	–0.047
			0.028	–0.007		0.002		
11 – $Fe^{III}O^-$	3	1.208	-0.001	0.863	–0.006	–0.003	0.863	–0.069
12 – $Fe^{III}OH^-$	2	0.801	0.010	0.115	–0.016	0.009	0.110	-0.067

Table 6. Geometries of the various models with an axial Cys ligand.

Model	spin state	Fe–S	Fe–N_{Por}	Fe–$N_{Por,av}$	Fe–O	O–O	O–H	Fe–O–O	Fe outp
1 – $Fe^{III}H_2O$	**2**	219.8	201.1–202.8	201.5	227.5		97.3		–13.8
	6	229.6	209.7–211.2	210.4	372.7		97.2		–51.7
2 – Fe^{III}	**6**	230.1	209.8–210.5	210.2					–49.8
3 – Fe^{II}	**5**	238.8	215.7–217.4	216.6					–66.0
4 – $Fe^{III}O_2^-$	**os 1**	232.3	201.5–203.2	202.3	195.0	130.7		119.5	–4.3
5 – $Fe^{II}O_2^{2-}$	**2**	240.2	201.2–203.2	202.2	199.2	132.5		120.6	–4.0
6 – $Fe^{III}OOH^-$	**2**	234.1	201.9–203.6	202.6	187.8	146.0	97.5	116.6	1.2
7 – Compound I	**2**	260.7	201.3–202.8	202.0	162.9				15.8
	4	261.9	201.6–202.3	202.0	162.9				16.4
	ε = 80	**256.2**	201.5–202.0	201.7	164.3				16.3
8 – $Fe^{IV}OH^-$	3	227.9	201.1–202.6	201.7	182.7		97.4		–0.6
9 – $Fe^{III}CH_3OH$	**2**	220.4	200.9–202.2	201.6	224.1		97.2		–11.9
	6	229.9	209.2–212.0	210.3	404.9		97.3		–51.1
10 – $Fe^{III}H_2O_2$	2	219.1	200.0–203.1	201.5	232.2	145.6	97.7		–15.2
							98.6		
	6	229.9	209.3–212.0	210.3	338.8	145.3	97.6		–49.5
							98.6		
11 – $Fe^{III}O^-$	3	246.0	202.8–203.0	202.9	166.6				7.0
12 – $Fe^{III}OH^-$	2	234.1	202.2–203.1	202.7	188.4		97.2		1.2

Table 7. Geometries of the various models with an axial His+Asp ligand. If not otherwise stated (H on His), it is assumed that the shared proton is located on Asp (His+HAsp).

Model	spin state	Fe–N_{His}	Fe–N_{Por}	Fe–$N_{Por,av}$	Fe–O	O–O	O–H	Fe–O–O	Fe outp
1– $Fe^{III}H_2O$	2	188.1	200.5–202.4	201.5	215.1		97.4		–12.3
	ε = 80	191.3	200.9–201.7	201.3	209.7		97.4		–9.4
2 – Fe^{III}	4	202.5	201.6–201.9	201.8					–29.7
	6	197.9	208.7–209.8	209.3					–48.8
	H on His	201.1	208.2–209.0	208.5					–46.4
3 – Fe^{II}	5	207.8	214.3–214.8	214.6					–59.1
	H on His	210.4	213.5–214.0	213.6					–55.4
4 – $Fe^{III}O_2^-$	os 1	201.2	201.5–202.8	202.1	190.1	130.4		119.5	–2.8
	H on His	203.8	201.4–202.7	202.0	189.1	130.1		119.4	–1.6
5 – $Fe^{II}O_2^{2-}$	2	209.6	201.4–202.8	202.1	196.7	132.9		119.9	–1.7
	ε = 80	206.3	201.2–203.0	202.1	189.6	135.9		121.2	–0.3
	H on His	211.1	201.5–202.7	202.1	195.8	132.8		119.8	–0.8
6 – $Fe^{III}OOH^-$	2	202.0	201.5–203.3	202.5	183.8	145.3	97.6	117.2	–0.6
	H on His	204.2	201.4–203.3	202.4	182.7	145.1	97.6	117.2	–1.1
7 – Compound I	2	216.1	202.4–202.7	202.5	163.3				10.2
	ε = 80	208.2	202.2–202.4	202.3	165.3				8.0
	H on His	213.7	202.4–202.6	202.5	163.8				8.6
	4	215.7	202.5–202.6	202.5	163.4				10.0
	ε = 80	207.9	202.1–202.3	202.2	165.3				7.8
	H on His	212.1	202.2–202.6	202.4	164.0				8.0
8 – $Fe^{IV}OH^-$	3	194.3	200.2–201.5	200.8	179.8		97.4		1.0
	ε = 80	200.4	199.3–201.2	200.4	180.6		97.5		2.0
9 – $Fe^{III}CH_3OH$	2	188.8	200.8–202.4	201.4	214.0				–10.4
10 – $Fe^{III}H_2O_2$	2	187.5	200.0–202.5	201.1	222.0	145.6	97.8, 98.6	115.5	–14.2
11 – $Fe^{III}O^-$	3	210.7	202.6–202.7	202.6	164.8				7.0
12 – $Fe^{III}OH^-$	2	205.2	202.0–202.5	202.2	184.3		97.2		1.1

Table 8. Geometries of the various models with an axial His ligand.

Model	spin state	Fe–N	Fe–N_{Por}	Fe–$N_{Por,av}$	Fe–O	O–O	O–H	Fe–O–O	Fe outp
1 – $Fe^{III}H_2O$	2	195.9	200.4–201.7	201.0	206.2		97.5		–7.4
	4	220.8	200.2–200.9	200.6	243.1		97.1		–10.3
2 – Fe^{III}	4	215.6	200.1–200.4	200.3					–22.9
	6	210.7	206.4–207.0	206.7					–38.8
3 – Fe^{II}	3	231.7	201.6–202.0	201.9					–13.4
	5	220.5	208.4–210.6	209.4					–30.4
	ε = 80	217.5	209.0–211.1	210.0					–36.2
4 – $Fe^{III}O_2^-$	os 1	212.2	201.2–202.7	201.9	187.3	129.0		118.9	2.1
	ε = 80	204.3	200.9–202.3	201.6	189.6	130.9		119.3	0.8
5 – $Fe^{II}O_2^{2-}$	2	201.0	201.5–202.9	202.2	193.3	132.4		118.8	1.4
	ε = 80	207.5	201.4–203.0	202.2	189.7	135.4		121.0	0.6
6 – $Fe^{III}OOH^-$	2	211.3	201.1–203.1	202.3	180.5	144.7	97.5	115.6	4.7
7 – Compound I	2	216.9	202.3–202.7	202.5	163.1				8.5
	4	216.7	202.3–202.7	202.5	163.1				8.4
	ε = 80	213.1	202.1–202.2	202.2	164.2				9.4
8 – $Fe^{IV}OH^-$	3	207.9	198.1–201.4	200.3	175.9		97.6		6.9
9 – $Fe^{III}CH_3OH$	2	196.7	200.7–201.7	201.0	204.7		97.3		–5.4
	4	222.0	200.3–201.0	200.7	238.0		97.1		–8.6
10 – $Fe^{III}H_2O_2$	2	195.4	199.8–201.9	200.7	209.1	145.4	98.0, 97.8	117.9	–8.2
11 – $Fe^{III}O^-$	3	221.5	202.3–202.6	202.4	162.9				11.8
	ε = 80	216.5	202.1–202.4	202.2	164.2				11.2
12 – $Fe^{III}OH^-$	2	210.9	201.7–202.6	202.1	180.8		97.3		4.8

Table 9. Spin densities of the various models with a Cys ligand.

	Spin state	Fe	S	O	$N_{Por,av}$	Cys	O–ligand	Porf
1 – $Fe^{III}H_2O$	2	0.979	0.099	–0.005	–0.017	0.098	–0.003	–0.074
2 – Fe^{III}	6	4.033	0.473	–	0.097	0.491	–	0.477
3 – Fe^{II}	5	3.663	0.148	–	0.031	0.159	–	0.178
4 – $Fe^{III}O_2^-$	os1	–1.051	–0.090	0.433		–0.089		
				0.613	0.019		1.046	0.094
5 – $Fe^{II}O_2^{2-}$			–0.009	0.422	–0.025	–0.009		–0.695
	2	0.753		0.530			0.952	
				0.280	–0.005			–0.110
	ε=80	0.667	0.000	0.163		0.000	0.443	
6 – $Fe^{III}OOH^-$				0.098	–0.014			–0.087
	2	0.932	0.055	0.002		0.055	0.101	
7 – Compound I	2	1.239	–0.750	0.858	–0.059	–0.761	0.858	–0.336
	ε = 80	1.401	–0.622	0.727	–0.089	–0.634	0.727	–0.494
	4	1.145	0.719	0.883	0.054	0.731	0.883	0.241
	ε = 80	1.273	0.579	0.762	0.072	0.591	0.762	0.373
8 – $Fe^{IV}OH^-$	3	1.740	0.196	0.187	–0.033	0.207	0.188	–0.135
	ε = 80	1.918	0.068	0.137	–0.040	0.073	0.139	–0.131
9 – $Fe^{III}CH_3OH$	2	0.994	0.088	–0.001	–0.018	0.087	–0.001	–0.080
10 – $Fe^{III}H_2O_2$	2	0.982	0.096	–0.005	–0.017	0.094	–0.003	–0.073
				0.000				
11 – $Fe^{III}O^-$	3	1.225	–0.013	0.876	–0.006	–0.011	0.876	–0.090
	ε = 80	1.401	–0.024	0.717	–0.014	–0.022	0.717	-0.096
12 – $Fe^{III}OH^-$	2	0.949	0.061	0.085	–0.015	0.060	0.081	-0.090

Table 10. Spin densities of the various models with a His+Asp ligand.

	Spin state	Fe	N_{His}	O	$N_{Por,av}$	His	O–ligand	Acetate	Porf
1 – $Fe^{III}H_2O$	2	0.996	0.001	–0.003	–0.019	0.062	–0.003	–0.001	–0.055
2 – Fe^{III}	6	4.176	0.176		0.111	0.261		0.002	0.562
	H on His	4.187	0.143		0.117	0.196		0.014	0.603
3 – Fe^{II}	5	3.732	0.036		0.032	0.067		0.001	0.201
	H on His	3.735	0.032		0.032	0.058		0.001	0.206
4 – $Fe^{III}O_2^-$	os1	1.085	–0.007	–0.408 –0.623	–0.022	0.020	–1.031	0.000	–0.074
	H on His	1.105	–0.011	–0.411 –0.632	–0.023	0.010	–1.043	0.000	–0.071
5 – $Fe^{II}O_2^{2-}$	2	0.049	–0.002	0.454 0.532	0.002	–0.003	0.986	0.000	–0.032
	ε = 80	0.267	–0.005	0.432 0.377	0.003	–0.006	0.809	0.000	–0.070
	H on His	0.038	–0.002	0.452 0.537	0.002	–0.002	0.989	0.000	–0.025
6 – $Fe^{III}OOH^-$	2	0.914	–0.014	0.137 0.008	–0.015	0.008	0.146	0.000	–0.068
	H on His	0.909	–0.017	0.144 0.008	–0.014	0.001	0.153	0.000	–0.063
7 – Compound I	2	1.163	0.018	0.914	–0.057	–0.661	0.914	–0.001	–0.416
	ε = 80	1.308	–0.052	0.808	–0.155	–0.043	0.808	–0.001	–1.073
	H on His	1.168	–0.036	0.922	–0.085	–0.026	0.922	–0.463	–0.600
	ε = 80	1.293	–0.045	0.817	–0.150	–0.038	0.817	–0.002	–1.070
	4	1.134	–0.050	0.921	0.055	0.631	0.921	0.001	0.314
	ε = 80	1.227	0.010	0.826	0.138	0.024	0.826	0.000	0.922
	H on His	1.120	0.006	0.934	0.094	0.013	0.934	0.371	0.561
	ε = 80	1.225	0.006	0.827	0.135	0.015	0.827	0.002	0.933
8 – $Fe^{IV}OH^-$	3	1.815	0.019	0.194	–0.038	0.011	0.196	0.000	–0.022
	ε = 80	1.917	–0.020	0.153	–0.039	0.022	0.156	–0.001	–0.095
9 – $Fe^{III}CH_3OH$	2	1.006	–0.005	–0.002	–0.020	0.052	–0.001	–0.001	–0.06
10 – $Fe^{III}H_2O_2$	2	0.991	0.002	–0.008 0.001	–0.018	0.064	–0.006	0.000	–0.049
11 – $Fe^{III}O^-$	3	1.187	–0.020	0.898	–0.005	–0.010	0.898	0.000	–0.075
	ε = 80	1.340	–0.021	0.753	–0.012	–0.011	0.753	0.000	–0.081
12 – $Fe^{III}OH^-$	2	0.971	–0.020	0.114	–0.017	–0.018	0.109	0.000	-0.062

Table 11. Spin densities of the various models with a His ligand.

	Spin state	Fe	N_{His}	O	$N_{Por,av}$	His	O–ligand	Porf.
1 – $Fe^{III}H_2O$	2	1.054	–0.037	–0.005	–0.023	–0.012	–0.004	–0.038
2 – Fe^{III}	6	4.187	0.088	–	0.129	0.108	–	0.708
3 – Fe^{II}	5	3.796	0.032	–	0.042	0.044	–	0.159
4 – $Fe^{III}O_2^-$	os1	1.188	–0.007	–0.449	–0.024	0.004	–1.123	–0.070
				–0.674				
	ε = 80		–0.018	–0.424	–0.024	–0.001	–1.022	–0.066
		1.088		–0.598				
5 – $Fe^{II}O_2^{2-}$	2	0.021	–0.002	0.445	0.002	–0.003	0.996	–0.014
				0.551				
	ε = 80		–0.004	0.438		–0.004		–0.053
		0.218		0.401	0.003		0.840	
6 – $Fe^{III}OOH^-$	2	0.960	–0.015	0.105	–0.016	0.006	0.099	–0.065
				–0.009				
7 – Compound I	2	1.138	–0.034	0.949	–0.097	–0.028	0.949	–1.059
	ε = 80	1.278	–0.040	0.824	–0.128	–0.032	0.824	–1.070
	4	1.091	0.004	0.949	0.128	0.008	0.949	0.952
	ε = 80	1.221	0.002	0.829	0.121	0.009	0.829	0.941
8 – $Fe^{IV}OH^-$	3	1.885	–0.024	0.183	–0.033	–0.013	0.188	–0.060
9 – $Fe^{III}CH_3OH$	2	1.054	–0.036	–0.001	–0.023	–0.012	–0.001	–0.040
10 – $Fe^{III}H_2O_2$	2	1.055	–0.039	–0.008	–0.023	–0.019	–0.007	–0.029
				–0.001				
11 – $Fe^{III}O^-$	3	1.171	–0.013	0.893	–0.003	–0.010	0.893	–0.054
	ε = 80	1.330	–0.018	0.753	–0.010	–0.012	0.753	–0.072
12 – $Fe^{III}OH^-$	2	0.933	–0.011	0.135	–0.014	–0.010	0.129	-0.052

Table 12. Reaction energies (in kJ/mole; one decimal) and reduction potentials (V; two decimals) of the investigated complexes optimised in vacuum and in water solution.

Reaction	Cys		Tyr		Tyr+Arg		His+Asp		His	
	ε = 1	ε = 80	ε = 1	ε = 80	ε = 1	ε = 80	ε = 1	ε = 80	ε = 1	ε = 80
1 → 2 + H_2O	14.6	–7.8	–12.5	–28.7	0.9	–24.8	25.4	9.4	39.4 27.5[a]	15.9
2 + e^- → 3	–2.82	–0.95	–2.66	–0.96	0.38	–0.71	–2.01 –1.61[c]	–0.58 –0.40[c]	0.90 0.68[a]	–0.28
3 + O_2 → 4	–36.8	–53.1	–17.7	–41.0	–5.8	–37.9	–28.2 –27.4[c]	–50.9 –50.3[c]	–19.2 –17.4[a]	–48.1
4 + e^- → 5	–6.65	–1.72	–6.39	–1.67	–3.67	–1.76	–5.84 –5.47[c]	–1.44 –1.28[c]	–3.27	–1.18
5 + ImH^+ → 6 + Im	–824.2	–138.6	–810.8	–146.3	–544.9	–144.6	–752.5 –717.7[c]	–115.9 –101.1[c]	–508.6	–51.8
4+ImH^++e^-→6+Im	1.89	–0.29	2.01	–0.15	1.98	–0.27	1.96 1.97[c]	–0.24 –0.24[c]	2.01	–0.65
6+ImH^+→7+H_2O+Im	–439.1	–64.1	–424.1	–65.4	–133.4	–46.3	–364.4 –364.4[c]	–31.4 –26.5[c]	–107.0	–61.5
7 + CH_4 → 8 + $CH_3^•$	88.0	91.0	106.7 98.8[b]	120.1	90.8	101.7	89.2	98.7	104.5	114.1
8 + $CH_3^•$ → 9	–268.9	–256.6	–270.5	–269.4	–282.9	–264.0	–318.9	–324.0	–296.4 –306.2[a]	–282.6
7 + CH_4 → 9	–180.9	–166.7	–163.8	–149.3	–192.1	–162.3	–229.7	–225.2	–191.9 –202.1[a]	–168.5
9 → 2 + CH_3OH	39.8	26.1	15.2	9.7	32.3	11.1	89.0	89.6	70.2 56.5[a]	49.7
9+H_2O→1+CH_3OH	25.3	33.9	27.8	38.4	31.4	35.8	63.6	80.2	30.8 29.0[a]	33.8
2 + H_2O_2 → 10	–21.8	4.2	8.8	30.6	19.6	46.5	–25.4	–2.2	–27.5 –4.0[a]	–2.8
10+Im → 6 + ImH^+	417.9	–3.0	378.9	–29.2	89.7	–56.1	345.5	–34.4	71.2	–20.4
2 + HO_2^- → 6	–188.9	–45.9	–197.4	–45.6	–475.7	–56.1	–264.9 –304.1[c]	–83.6 –101.4[c]	–541.3 –517.8[a]	–70.3
7 + e^- → 11	–2.05	–0.08	–1.85 –1.91[b]	–0.11	1.27	0.33	–1.17	0.33	1.63	0.51
11 + e^- + 2ImH^+ → 2 + 2Im + H_2O	7.28	0.85	7.15	0.87	4.15	0.55	6.39	0.39	3.40 3.64[a]	0.04
8 + e^- → 12	–2.11	–0.15	–2.00	–0.21	0.97	0.06	–1.35	0.27	1.58	0.58
11 + ImH^+ → 8 + Im	–466.6	–48.4	–427.9 –441.8[b]	–21.1	–142.7	2.7	–379.3	–0.3	–94.2	32.2
12+ ImH^+ → 1 + Im	–454.4	–39.8	–442.8	–54.1	–164.7	–25.0	–392.6	–20.7	–119.9 –131.5[a]	5.0
7+H_2O_2 →2+H_2O+O_2	–161.9	–139.3	–168.5	–138.3	–180.8	–147.5	–160.6 –145.0[c]	–134.3 –122.0[c]	–141.6 –165.5[a]	–117.5
10 → 7 + H_2O	–21.2	–67.1	–45.1	–94.6	–44.7	–99.7	–18.9	–65.7	–35.7	–82.0
10 → 8 + $OH^•$	89.0	61.3	84.6	64.0	69.2	40.5	93.4	71.5	91.9	70.7

[a] Intermediate-spin state.
[b] The perpendicular conformational.
[c] The HisH+Asp conformation.

Figure 1. The reactions involved in the cycles of cytochrome P–450, peroxidase, and catalase.

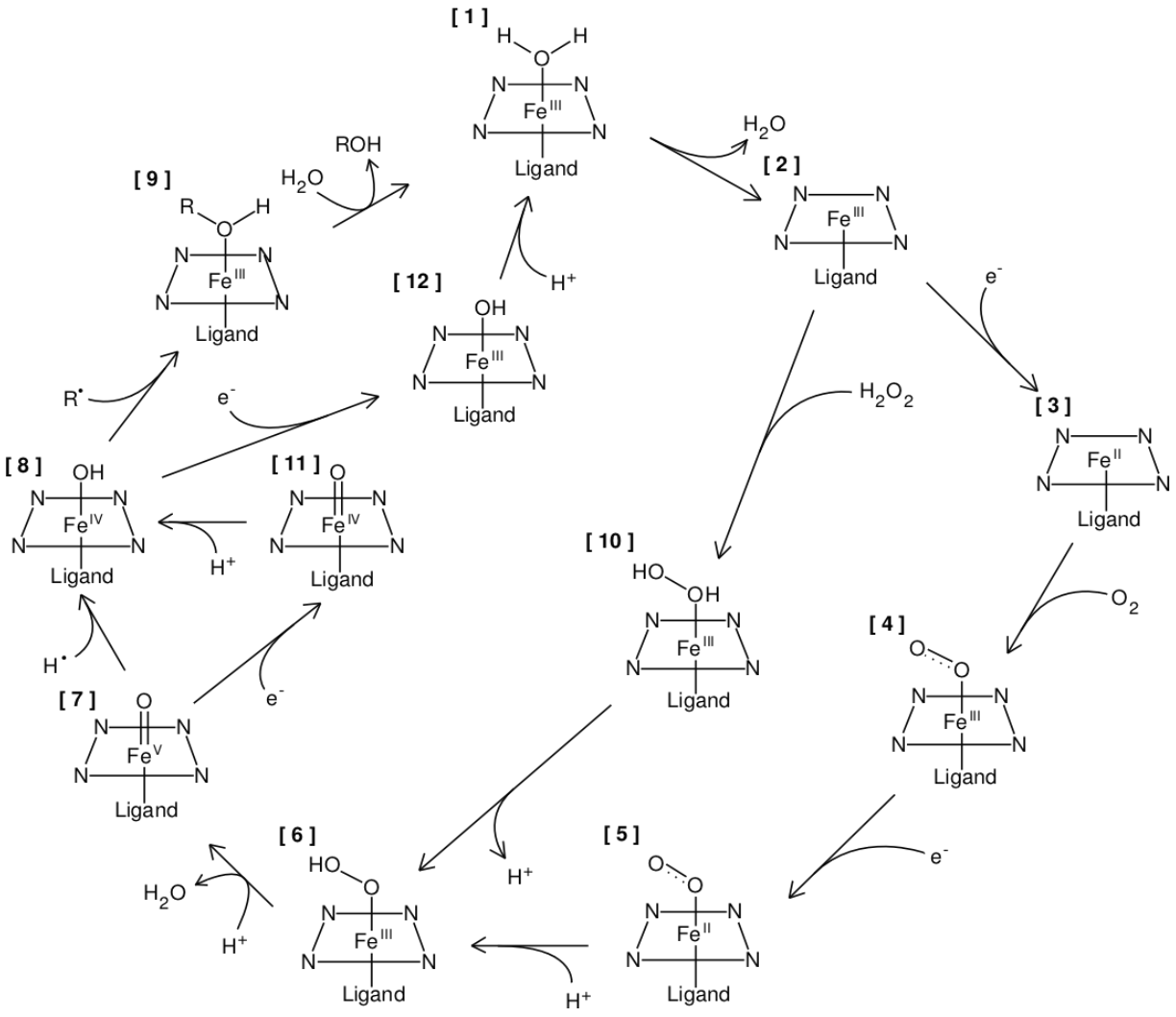

Figure 2. A comparison of the two orientations of the Tyr ring for compound I (**7**), parallel (a) and perpendicular (b).

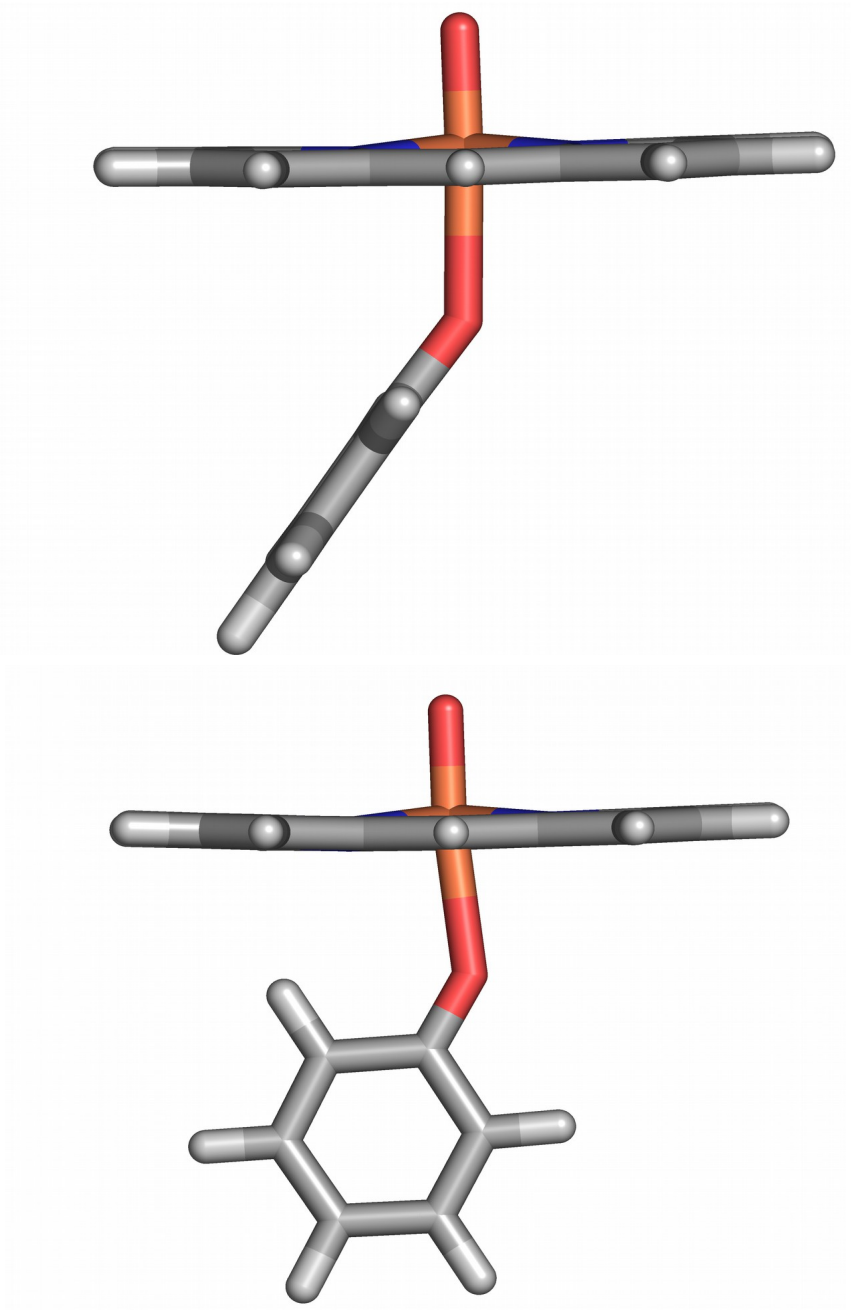

Figure 3. The optimised structures of all optimised Tyr complexes (**1**–**12**) in their lowest spin states.

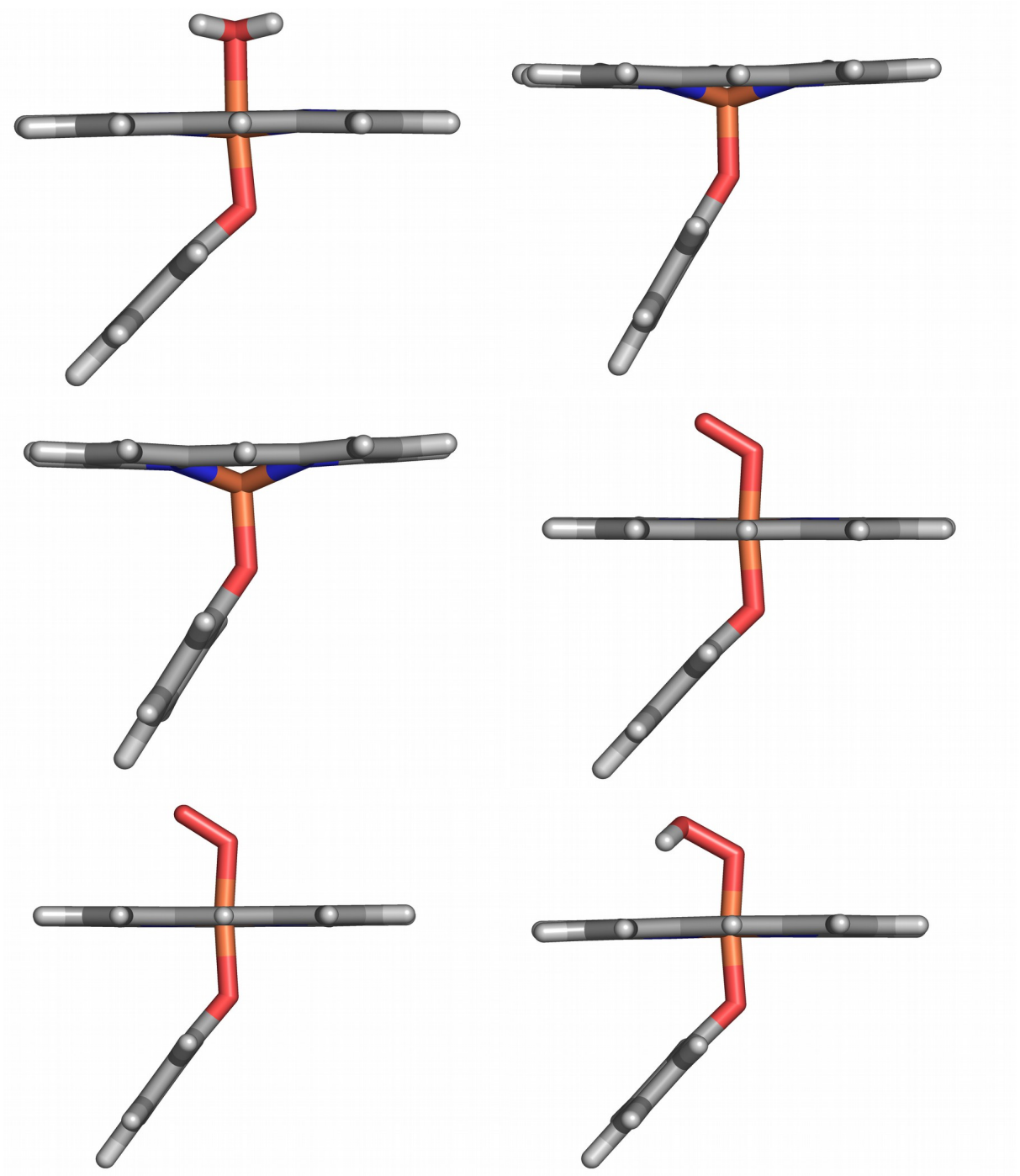

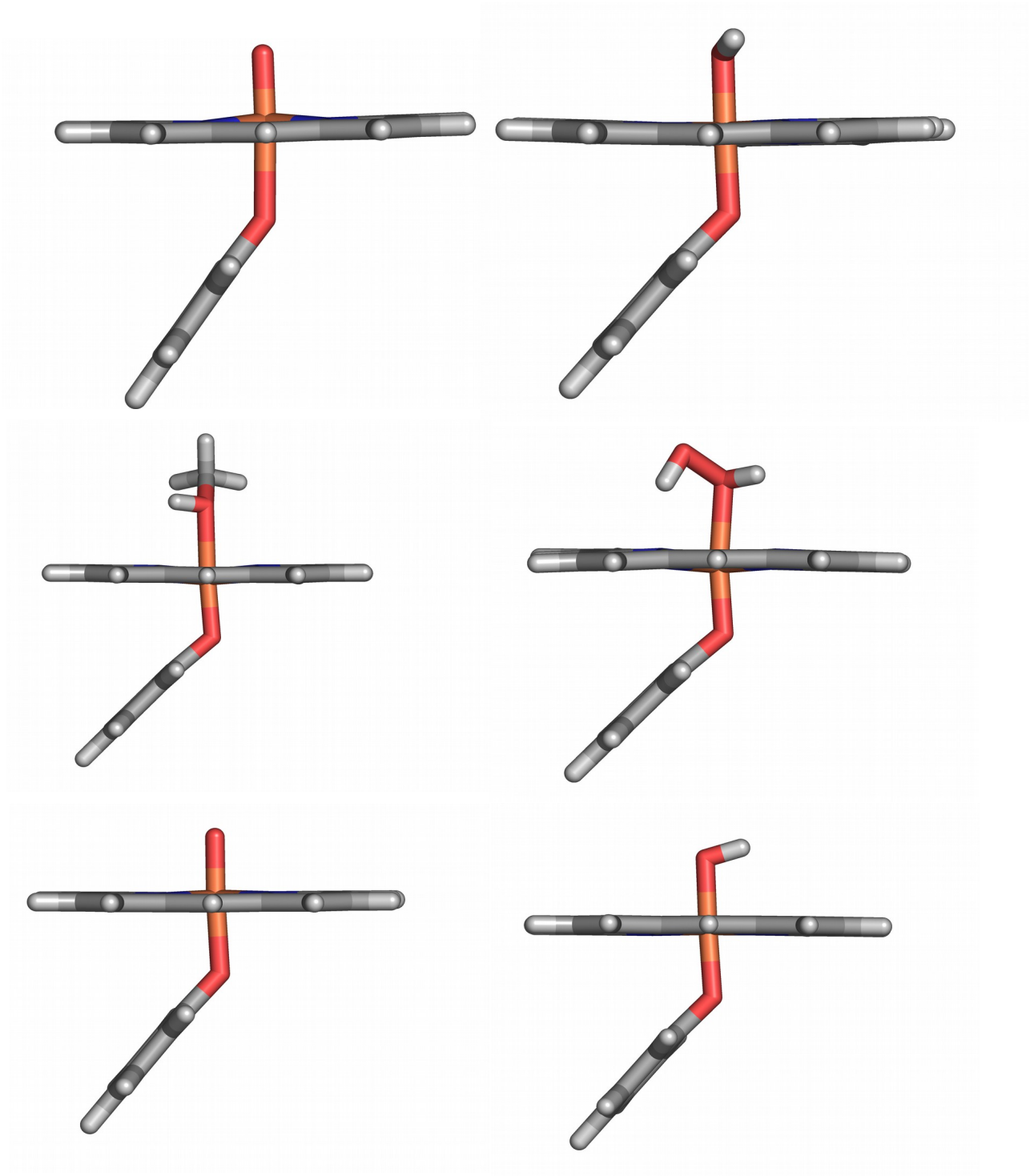

Figure 4. The Tyr+Arg structure of compound I (**7**) in the doublet state.

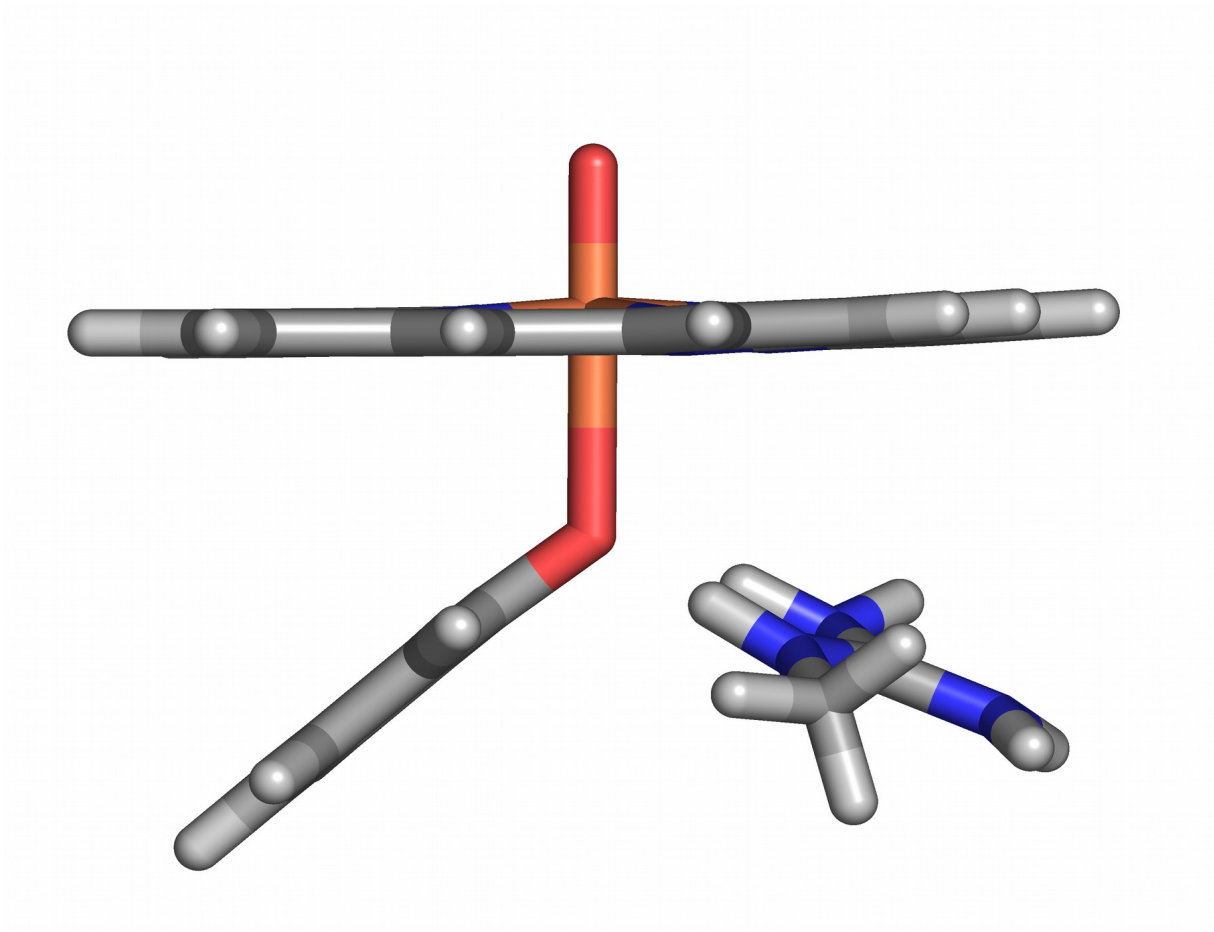

Figure 5. The His+Asp structure of compound I (**7**) in the quartet state, with the proton either on Asp (a) or on His (b).

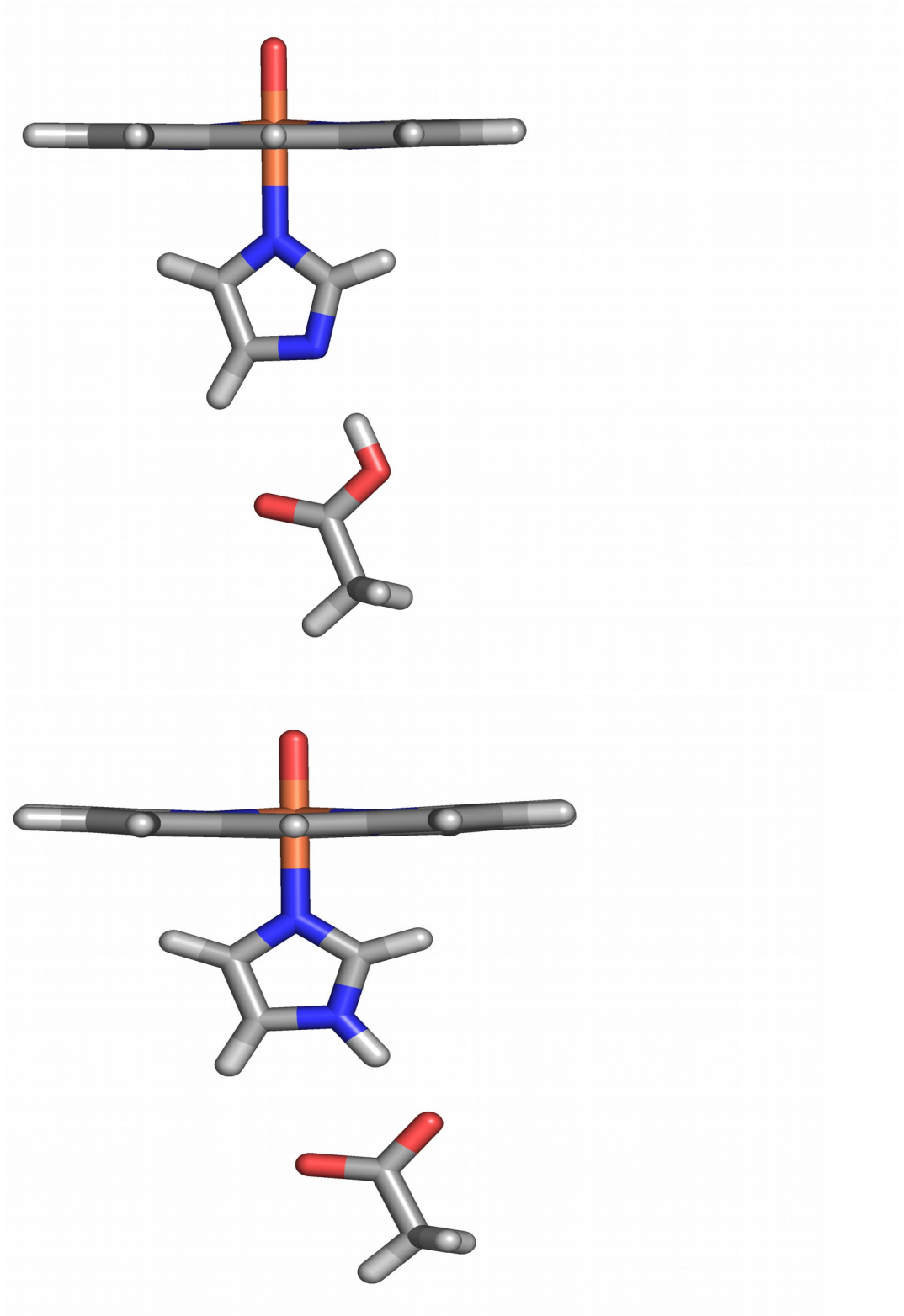

Figure 6. The optimised structures of all Cys and His complexes (**1**–**12**) in their lowest spin states.